Title: Symplastic intercellular connectivity regulates lateral root patterning

Authors: Yoselin Benitez-Alfonso[1,3*], Christine Faulkner[1,4], Ali Pendle[1], Shunsuke Miyashima[2], Ykä Helariutta[2], Andrew Maule[1].

Affiliations:

[1] John Innes Centre, Norwich Research Park, Norwich, Norfolk NR4 7UH, UK.

[2] Plant Biology, Viikinkaari 1 (PL 65), University of Helsinki, Helsinki 00014, Finland.

[3] Present address: Centre for Plant Sciences, School of Biology, University of Leeds, Leeds, LS2 9JT, UK.

[4] Present address: Department of Biological and Medical Sciences, Oxford Brookes University, Gipsy Lane, Oxford, OX3 0BP, UK.

Contact:

*Correspondence to Yoselin Benitez-Alfonso

email: y.benitez-alfonso@leeds.ac.uk

Phone: (+44)0113 34 33103

Running title: Symplastic communication controls root development

Summary: Cell-to-cell communication coordinates the behavior of individual cells to establish organ patterning and development. While mobile signals are known to be important in lateral root development, the role of plasmodesmata (PD) mediated transport in this process has not been investigated. Here we show that changes in symplastic connectivity accompany and regulate lateral root organogenesis in Arabidopsis. This connectivity is dependent upon callose deposition around PD affecting molecular flux through the channel. Two Plasmodesma-localized β-1,3 glucanases (PdBGs) were identified that regulate this process. Callose accumulation, as well as the number and

distribution of lateral roots, was altered in mutants and over-expression lines for the PdBG genes. The fundamental role of PD-associated callose in these processes was illustrated by the induction of similar phenotypes in lines with altered callose turnover. Our results show that regulation of callose and cell-to-cell connectivity is critical in determining the pattern of lateral root formation, which influence root architecture and optimal plant performance.

Highlights

- Changes in cell-to-cell connectivity accompany lateral root (LR) formation.
- A family of beta-1,3-glucanases controls callose deposition in the nascent LR.
- Modifying PD aperture by altering callose degradation influences LR density.
- Ectopic callose deposition induces the formation of clustered primordia.

Introduction: The initiation of lateral root primordia (LRP) characterizes post-embryonic root development. This process uses environmental information to specify the relative positioning of primordia in order to maximise the potential for nutrient uptake. Lateral root emergence and extension then delivers an increase in root functional capacity underpinning increased plant growth (Peret et al., 2009; De Smet et al., 2006; Benkova and Bielach, 2010).

The molecular mechanisms that determine lateral root (LR) architecture have significant agronomic relevance but remain poorly understood. Different from the primary root meristem, secondary meristems are initiated *de novo* from xylem-pole pericycle (XPP) cells in the differentiation zone of the primary root. This process involves multiple steps of cellular re-definition and cell proliferation that have been classified into seven stages (I to VII; graphical abstract (Malamy and Benfey, 1997). Interconnected signaling pathways involving both hormone (auxin/cytokinin) transport and Auxin/Indole-3-acetic acid proteins (Aux/IAA) have been shown to regulate the expression of genes required during specification, de-differentiation and emergence of the lateral meristems (Aloni et al.,

2006; De Rybel et al., 2010; De Smet et al., 2010; Lucas et al., 2008; Moreira et al., 2013; Van Norman et al., 2011; Muraro et al., 2013). Oscillating auxin maxima in the basal meristem and, presumably, the intercellular transport of other mobile signals (Van Norman et al., 2011; De Smet et al., 2010; Moreno-Risueno et al., 2010) determines the characteristic spatial patterning of LRs, i.e. a regular distribution along the main root axis, oriented left-right in an alternating pattern.

The intercellular symplastic movement of signaling molecules through plasmodesmata (PD) determines embryonic cell fate and post-embryonic organ development (Xu et al., 2011; Xu and Jackson, 2010; Kim et al., 2002; Nakajima et al., 2001). Regulation of PD transport can be controlled through the accumulation of the β-1,3 glucan callose in the surrounding wall causing a constriction of the symplastic channel (Zavaliev et al., 2011). Callose turnover at PDs affects both targeted molecular transport (dependent on proteins and co-factors capable of modifying PD aperture) and non-targeted molecular flux (diffusion of small molecules such as GFP) (Vaten et al., 2011; Rinne et al., 2011; Guseman et al., 2010; Benitez-Alfonso et al., 2009). This regulatory mechanism plays a key role in a plethora of developmental processes including the specification of stomatal complexes, dormancy release prior to flowering, the maintenance of apical meristems, and during the sink-source transition (Guseman et al., 2010; Levy et al., 2007b; Vaten et al., 2011; Rinne et al., 2011). It also regulates plant responses to biotic and abiotic stresses (Benitez-Alfonso et al., 2009; Benitez-Alfonso et al., 2010; Levy et al., 2007a; Lee et al., 2011). In spite of the evidence that PD are dynamic structures and crucial to plant development and responses our understanding of the mechanics of PD function remains poor. Recently, significant progress has been made in the identification of novel PD proteins through genetic or proteomic screens (Bayer et al., 2006; Fernandez-Calvino et al., 2011; Simpson et al., 2009; Thomas et al., 2008; Vaten et al., 2011). These studies have identified proteins involved directly in callose synthesis and degradation (callose synthases, CALS and β-1,3 glucanases, BG) or indirectly modifying callose deposition (e.g. PD-callose binding protein, PDCB) as

PD components (Vaten et al., 2011; Fernandez-Calvino et al., 2011; Levy et al., 2007a; Simpson et al., 2009).

The importance of mobile factors (hormones, peptides, miRNAs, etc) in lateral root initiation and emergence is well recognized (De Smet et al., 2008; De Smet et al., 2010; Marin et al., 2010; Meng et al., 2012; Moreno-Risueno et al., 2010; Peret et al., 2012). It has been shown that mis-regulated PD connectivity, affecting the movement of non-cell autonomous factors and the downstream processes they trigger, can have a negative impact on the development of apical meristems and meristemoids (Guseman et al., 2010; Benitez-Alfonso et al., 2009; Kim et al., 2003; Nakajima et al., 2001; Rinne et al., 2011; Van Norman et al., 2011; Vaten et al., 2011; Xu et al., 2011). However, the role of symplastic transport in the formation of lateral root meristems has not yet been investigated. In this paper, we show that symplastic connectivity is critical for both the initiation and positioning of LR meristems, and that this connectivity is regulated by PD-associated glucanases concomitant with callose as a regulator of symplastic molecular flux through PD.

Results

Symplastic connectivity is regulated during lateral root development

To address the temporal and spatial regulation of cell-to-cell connectivity during primordia development, we used stable transgenic lines expressing reporters for GFP diffusion. For the purpose of this study we divided mature roots into three main regions: meristem (where cell division occurs), basal meristem (from the end of cell division to the first root hair, containing the region of LR priming), and lateral root forming zone (LR forming zone; containing stages I-VII and emerged primordia as defined in graphical abstract and other publications) (Fig.1**A**) (Malamy and Benfey, 1997). GFP expressed under the control of the *SUC2* (*SUCrose-proton symporter* 2) promoter (active in phloem companion cells, (Truernit and Sauer, 1995)) diffuses freely across all cell layers in the meristem (Stadler et al., 2005; Benitez-Alfonso et al., 2009). In the basal meristem and early LR forming region of 6 day old roots, we detected GFP signal in the stele, endodermis, cortex and epidermis suggesting

that symplastic connectivity between the phloem and the outer cell layers is maintained in this region (Fig. 1**B**). In contrast, GFP movement was differentially regulated in the LR forming zone (Fig. 1**C**-**G**). Proximal to stage II and III primordia, GFP movement was reduced but still diffused to pericycle cells, into the primordium and the endodermis (Fig. 1**C-D**). However, p*SUC2*-expressed GFP was excluded from stage IV-V primordia (notice that diffusion is still detectable in neighboring pericycle cells, Fig. 1**E**-**F**) and fluorescent signal in the new LR was only restored when a new functional vascular system was formed (Fig. 1**G**).

The results from the analysis of p*SUC2*-GFP plants suggest a block in post-phloem symplastic transport in late stages of primordia development; however, molecules produced within the primordium might have a different fate. To investigate this aspect, we generated transgenic plants expressing cytoplasmic GFP under the control of the *AUX1* promoter. We first confirmed *AUX1* expression in the basal meristem and LR forming zone using a translational fluorescent fusion. As described previously (Marchant et al., 2002), *AUX1* expression in the stele of the basal meristem zone gets restricted to the new LRP in the LR forming zone (Fig. S1**M-R**). Analysis of transgenic Col-0 plants expressing p*AUX1*-GFP confirmed stage IV and older LRP as domains with restricted connectivity to external cells. As for p*SUC2*-GFP, free GFP diffuses from the stele into the surrounding tissue in the basal meristem zone (compare Fig. S1**M** and Fig. 1**H**). Similarly, GFP produced in stage I-III primordia diffuses to neighboring tissues and cortical cells (Fig. 1**I**). However, GFP produced in stage IV and older primordia was retained within the primordium (Fig. 1**J-L**). Emerged primordia resembled the expression and diffusion profile of the main meristem (Fig. 1**M** and Fig. S1**S**).

Together these data point to a dynamic regulation of symplastic transport whereby positive cell-to-cell connectivity between pericycle cells and early stage primordia and the surrounding tissue becomes restricted in older LRP until emergence is completed.

Callose deposition at PD correlates with the formation of symplastic domains in lateral roots

Symplastic transport is regulated by the synthesis and degradation of callose at PD neck regions (Levy et al., 2007b; Vaten et al., 2011). This mechanism has been found to be important in the maintenance of symplastic permeability in apical meristems (Chen et al., 2009; Zavaliev et al., 2011; Benitez-Alfonso et al., 2009; Vaten et al., 2011). Therefore we analyzed the pattern of callose deposition during the formation of lateral meristems. Whole roots, excised from Col-0 seedling 6dpg, were fixed and immuno-labeled with callose antibodies. Secondary detection with the fluorophore Alexa 488 revealed that callose is deposited in the sieve plates, cell plates and in a punctate pattern in the cell-wall, reminiscent of PD localization (Fig. 2**A-G**). The analysis of multiple root sections revealed differences in the level of callose accumulated in the basal meristem and LR forming zones. Callose deposition was detected at low levels at PDs of the basal meristem zone and in non-lateral root regions within the LR forming zone (Fig. 2**A**). At early stages of lateral root development, callose gets deposited in the cell-plates and to moderate levels between cell layers (Fig. 2**B-C**). In contrast, in stage IV-V primordia PD and cell-wall labeling between the new meristem, the associated endodermal/cortical cell layer and the vasculature was significantly increased (Fig. 2**D**-**E**). This is coincident with the reduction in GFP diffusion observed in p*SUC2*-GFP and p*AUX1*-GFP plants (Fig. 1**E-F**, **J-L**). In the later stages, and during emergence, callose accumulation decreased but was still detected in the ruptured cortical and epidermal cells and in the new division walls within the new LR (Fig. 2**F-G**). To quantify these changes in callose accumulation, we stained a significant number (>20) of wild-type roots with the callose stain aniline blue and calculated the mean increment in fluorescence signal (mean gray value) in the cell-wall connecting the new lateral root and the overlying tissue (Fig. S2). This mean gray value was corrected by subtracting the background fluorescence contained in the same area in the wall opposite the primordium. The results support our previous conclusions i.e. total callose deposited around lateral roots increased progressively during development reaching a maximum in stage IV-V primordia (Fig. S2**F**).

In summary, changes in symplastic transport during LR development correlate with changes in callose deposited suggesting a role for callose turnover in regulating symplastic connectivity in LRP.

Identification of callose-degrading enzymes associated with lateral roots and PDs.

To identify proteins involved in the metabolism of PD-associated callose during LR organogenesis we examined PD proteomic data. Thirteen putative callose metabolic enzymes (1,3-β-D-glucanases and glucan synthases like, GSL) were represented in published PD proteomes (Bayer et al., 2006; Fernandez-Calvino et al., 2011). We used transcriptome data sets (compiled in the VisuaLRTC (Parizot et al., 2010)) to screen for genes involved in lateral root initiation (Table S1). This approach identified At3g13560 as a putative beta-1,3-glucanase preferentially expressed in the XPP (LR founder tissue) and that is induced by auxins in a SOLITARYROOT/IAA14-dependent manner. To confirm the expression of this gene in LRs, we analyzed transgenic plants expressing the β-glucuronidase gene (GUS) downstream of the native promoter (Fig. 3). At3g13560 (subsequently named *Plasmodesmal-localized Beta-Glucanase 1*; *PdBG1*) is expressed at very low levels in the pro-vasculature and vasculature of the basal meristem (Fig. 3**A,B**). Interestingly, *PdBG1* was induced in few pericycle cells associated with the xylem in the early LR forming zone which might correspond to sites of incipient primordia (Fig. 3**C**). Expression increased soon after LR specification reaching a maximum at stage III primordia (Fig. 3**D**-**F**). This expression pattern was confirmed using a gene-trap insertion line that carries GUS fused to the N-terminal portion of the protein (Fig. S3**A-E**).

To assess the cellular localization of PdBG1 we stably expressed an m-Citrine internal fusion (see experimental procedures for location of the m-Citrine) in Arabidopsis. In leaves and roots, PdBG1-mCitrine accumulated in punctate spots at the cell periphery reminiscent of PD localization (Fig. 3**G,L**). Confirming PD targeting, these spots co-localized with aniline blue stained-callose and with mCherry-PDCB1 (a PlasmoDesmal Callose Binding protein shown to associate with PD (Simpson et al., 2009)) (Fig. 3**H-I,M-N**). Supporting potential PdBG1 activity in callose degradation, wound-

induced callose was reduced in leaves over-expressing PdBG1 (PdBG1OE) relative to wild-type (Fig. 3**O-P**).

β-1,3-glucanases are encoded by a large gene family (Doxey et al., 2007). Phylogenetic analysis and expression profile data identified a close evolutionary relationship between *PdBG1* and the genes *At2g01630* (named *PdBG2*) and *At1g66250* (named *PdBG3*). PdBG2 and PdBG3 m-Citrine-tagged constructs also showed PD localization, suggesting that they all act to control callose deposition at PD (Fig. S3**G**-**L**). Moreover, microarray data indicates that *PdBG2* expression is high in XPP cells suggesting it might be involved in lateral root initiation (Table S1). To study *PdBG2* expression in lateral roots, we examined a line carrying a genetrap insertion in the first exon. *PdBG2* was up-regulated in the stele, the LRP and, sporadically, in the endodermis associated with putative lateral root-founder cells (Fig. S3**M-R**). This expression pattern partially overlaps with PdBG1 suggesting that they might be functionally redundant genes.

The data identifies 2 novel callose degrading enzymes (PdBG1 and PdBG2) that localize at PDs with expression patterns that implicate them in LR initiation and development.

PdBG1 and PdBG2 regulate callose deposition and symplastic connectivity during lateral root development.

To determine if PdBG1 and PdBG2 are involved in callose turnover during LR development we examined callose deposition in *pdbg1, pdbg2* and *pdbg1,2* double mutants. No significant difference was detected between single mutants and wild-type siblings but the double mutant displayed a visible increase in fluorescence in the stele and lateral root primordia upon aniline blue staining (Fig. S4**A-D**). Similar results were obtained using immunoassays: callose antibodies labeled more strongly *pdbg1,2* roots in comparison to wild-type siblings (Fig. 2**H-I**). The differences were more pronounced in the stele of the basal meristem (Fig. 2**H**) and pericycle associated with LRP (Fig. 2**I**). Relative quantification of the increment in fluorescence signal indicated that *pdbg1,2* accumulated about three

times more callose than wild-type roots (Fig. S4**F**). In comparison, aniline blue fluorescence was significantly reduced in PdBG1OE (about a two-fold decrease) supporting protein activity in callose degradation (Fig. S4**E-F**).

Excessive callose deposition has been found to obstruct PDs blocking symplastic intercellular transport (Guseman et al., 2010; Vaten et al., 2011). To test symplastic transport in *pdbg1,2*, we studied GFP diffusion in mutants expressing p*SUC2*-GFP. In the basal meristem and early LR forming zone, GFP expressed in the phloem of wild-type siblings was able to move symplastically into the endodermis and cortex (Fig.1**B** and Fig. 4**A,C**). Conversely, in *pdbg1,2* roots, GFP was retained in the phloem (Fig. 4**B**,**C**). This was consistent with the increase in stele-associated callose observed in *pdbg1,2* root (Fig. 2**H**). Excessive callose deposition has been shown to affect the transport of the SHORTROOT protein (SHR) from the stele to the endodermis (Vaten et al., 2011). In *pdbg1,2* mutants transformed with pSHR::SHR-GFP we could not detect changes in SHR-GFP transport relative to siblings in the wild-type background (Fig. 4**D-E**) consistent with the low level of expression detected for PdBG1 and PdBG2 in emerging LRP (Fig. 3**E-F**) .

Since the double mutant displayed a reduction in symplastic connectivity, overexpression will likely have the reverse effect. Supporting this hypothesis, we showed that mRFP, produced from bombarded mRFP cDNA, more frequently moved further (number of cells showing mRFP) in PdBG1OE leaves in comparison to wild-type (Fig. 4**F**). Moreover, symplastic diffusion of CFDA (carboxyfluorescein diacetate) in roots exposed for 5min to the dye, was enhanced in PdBG1OE stage IV-VI primordia in comparison to wild-type (Fig. 4**G**-**I**).

Together these results indicate that PdBGs are necessary and sufficient to regulate callose and intercellular transport during development of lateral root primordia.

Changes in callose accumulation and PD flux affect lateral root initiation and distribution.

The localization and pattern of expression for the PdBG proteins suggest that they might play a role in lateral root development. To further investigate this hypothesis, we studied the lateral root phenotype of PdBG mutants and over-expression lines. Lateral root density (number of LR initiation events per mm of root) has been used to characterize defects in LR development (Benkova and Bielach, 2010). *pdbg1*, *pdbg2* and double mutants, in both Col-0 and Ler backgrounds, showed an increase in the number of initiated primordia relative to wild-type roots (Fig. 5**A** and Fig. S5**A**). The effect was stronger in *pdbg1,2* double mutant roots, confirming that these genes have partially redundant functions.

Closer examination of mutant roots showed that primordia frequently formed adjacent to each other which occasionally led to the emergence of a fused LR (Fig. 5**B**). To investigate this phenotype we created transgenic plants expressing a reporter for *GATA23*, a gene that controls LR-founder cell specification (De Rybel et al., 2010). In wild-type roots, *GATA23* peaks of expression were regularly spaced which was coincident with the normal distribution of LRP along the main root (Fig. 5**C,** 6**B**). In contrast, *pdbg1,2* had extended domains of *GATA23* expression which correlated with the initiation of LR in clusters (Fig. 5**D**).

It has been reported that the relative position and distance between lateral roots are marked by periodic pulses of DR5 expression in the oscillatory zone (pre-branch sites) (Moreno-Risueno et al., 2010). Since *pdbg1,2* displayed altered callose deposition and symplastic transport in the basal meristem (which contains the oscillatory zone) and formed fused primordia, we investigated LR priming by expressing the reporter p*DR5*-3xVENUS-N7 (Brunoud et al., 2012) in wild-type and *pdbg1,2* roots. While the reporter was induced at regular intervals in the oscillatory zone of wild-type roots (Fig. 5**E**), priming sites seem clustered together in the mutant (Fig. 5**F**). *DR5* expression overlapped with *GATA23* in LRP and, as before, extended domains of *DR5* expression in *pdbg1,2* indicated disrupted primordia spatial patterning (compare panels in Fig. 5**E** and **F**).

Consistent with a role for PdBG in lateral root initiation, PdBG1OE showed the reciprocal effect: a significant decrease in lateral root density (Fig. 6**A**). In agreement with this observation, the distance between *GATA23*-marked initiation sites was larger in PdBG1OE when compared with wild-type siblings suggesting that primordia are spread more widely in this line (Fig. 6**B-C, F**).

Defects in lateral root initiation are often correlated with impaired maintenance of the apical meristem and/or altered emergence since these processes share some commonalities in their signalling pathways (Aloni et al., 2006; Lucas et al., 2008; Peret et al., 2009). To investigate the role of PdBGs in root meristem development and LR emergence, we quantified root meristem size and percentage of emergence in *pdbg1,2* and PdBG1OE lines. Although double mutant and over-expressors had opposite effect on callose and lateral root number they both showed a mild reduction in meristem size in comparison to wild-type and were similar in appearance at the whole plant scale (Fig. S5**B-C**). This suggests that these genes are not main regulators of apical meristem development. Supporting this conclusion, callose was deposited at similar levels in wild-type and *pdbg1,2* apical root meristem regions (Fig. S5**D-E**).

To complement our observations we examined the percentage of LR emergence in mutant and overexpressing lines. The percentage of emerged LR was similar in *pdbg1*, *pdbg2* single and double mutants and wild-type but increased in PdBG1OE (Fig. S6**A**). Increased emergence in PdBG1OE could be directly caused by ectopic expression of a cell-wall modifying enzyme (Swarup et al., 2008) or an indirect consequence of the reduction in primordia initiation (Lucas et al., 2008). To uncouple these developmental processes, we synchronized primordia initiation by applying a gravitropic stimulus to 3 days old roots. Primordia initiate synchronously 12h after root bending and fully emerge 48h post-gravistimulation (Peret et al., 2012). We could not detect differences in the percentage of 'emerging' primordia 42h post-gravistimulation between, either *pdbg1,2* or PdBG1OE and wild-type roots suggesting that emergence is not directly regulated by these genes (Fig. S6**B-C**).

The phenotypes described in mutant and over-expression lines suggest that PdBG1,2 are primarily involved in LR initiation and spatial patterning. To address if PdBG activity on callose degradation is directly responsible for these phenotypic defects, we examined LR density in a PDCB1 over-expression line. Ectopic expression of PDCB1 has been shown to decrease symplastic transport and increase callose deposition at PD neck regions (Simpson et al., 2009). We found that similar to *pdbg1,2,* PDCB1OE showed increased LR density (Fig. 6**A**) and neighboring primordia that corresponded with clustered sites of *GATA23* expression (Fig. 6**D-E**). This result provides independent evidence that links callose to the regulation of lateral root patterning.

To further demonstrate the importance of callose regulation in this process, we studied inducible transgenic lines expressing a mutated/activated version of PD-located CALS3 (cals3m). Induction of cals3m has been shown to modify PD-associated callose and symplastic transport within 48h (Vaten et al., 2011). To express this protein specifically in the XPP (LR competent tissue), we transformed an estradiol-inducible UAS promoter driving cals3m into the enhancer-trap line J0121 (Fig. 7**A;** Parizot et al., 2008). This construct was named J0121>>cals3m. In our conditions, 24 hours of estradiol treatment was sufficient to produce a significant amount of callose in the XPP (Fig. 7**B-C**). Lateral root density was analyzed in estradiol-treated and mock-treated lines 72h post-induction (48h after increase callose deposition was confirmed). As expected, the number of initiated primordia was significantly higher in induced J0121>>cals3m, consistent with a role for PD-associated callose in lateral root initiation (Fig. 7**D**). We used the GATA23 promoter to drive GUS expression in the callose inducible lines to monitor LR initiation. 48h estradiol induction of J0121>>cals3m induced the initiation of neighboring LRP and clusters reported by large domains of *GATA23* expression (Fig. 7**E-F**). This result confirms that callose regulation of intercellular connectivity between pericycle cells, founder cells and the neighboring tissue is important to establish lateral root patterning in Arabidopsis.

Discussion

Lateral root formation has been attributed to auxin gradients that trigger initiation events in the root pericycle. This causes re-differentiation of lateral root founder cells and the formation of new meristems. Mobile signals (including, but not restricted to auxins) have been proposed to play a role in the relative positioning of primordia and the emergence phase of lateral root development (De Smet et al., 2008; Peret et al., 2012; Moreno-Risueno et al., 2010; Van Norman et al., 2011; Marin et al., 2010; Meng et al., 2012). We have identified that symplastic domains are regulated around LRP, through a mechanism that involves the deposition of PD-associated callose. This process regulates intercellular signalling and is fundamental to the definition of LR spatial patterning.

Our data indicates that prior to and during LRP specification all cells are symplastically connected to the pericycle. Hence GFP diffuses readily through the cells of the stele and outer tissues (Fig.1). Following the first pericycle cell divisions, symplastic connectivity is reduced, which correlates with an increase in callose deposited around stage IV-V primordia. In agreement with our results, previous studies using dye loading experiments reported that symplastic continuity between the emerging primordia and the phloem of the primary root is lost and only re-established when a new phloem connection is formed (Oparka et al., 1995). The reasons behind this late down-regulation in symplastic transport might lie in the need to maintain water pressure (and tissue hydraulics) relevant during the emergence phase (Peret et al., 2012) but questions remain regarding the role of symplastic regulation early in LRP development.

PdBG1 and PdBG2 are novel PD-located callose degrading enzymes expressed in the stele and early stages primordia. PdBG1 and PdBG2 are induced in auxin-treated roots but not in the mutant *solitary root1*, suggesting that they are potential targets of the auxin signaling pathway that regulates lateral root initiation (Vanneste et al., 2005). Interestingly, PdBG orthologs in *Populus* are up-regulated during dormancy release suggesting a role for these enzymes in shoot meristem development (Rinne et al., 2011).

We demonstrated that symplastic connectivity in the basal meristem and lateral root-forming zone depend on PdBG1/PdBG2 activity. Moreover, these enzymes influence LR initiation and positioning. Double mutants *pdbg1,2,* are impaired in callose degradation, exhibit restricted PD transport higher LR density and distorted primordia patterning (Fig 2, 4, 5). LR phenotypes caused by the absence of PdBG1 and/or PdBG2 are associated with the function of these proteins during LR initiation and not emergence (Fig. S6). As expected, over-expression of PdBG1 produced the opposite effect with respect to LR density and patterning. Interestingly, the auxin-response factor DR5 is induced in neighboring pericycle cells in the basal meristem of *pdbg1,2* which implicates symplastic connectivity in the formation of pre-branching sites. Temporal and spatial distribution of LRs is established by the oscillating expression of genes that determine periodic root branching and bending (Moreno-Risueno et al., 2010). Cell-to-cell connectivity might regulate the mobility of factors that originate in primed cells to repress lateral root initiation in adjacent pericycle cells or the transport of a LR inhibitory signal from neighboring tissues into the XPP (Traas and Vernoux, 2010). Both models predict an increase in the number of lateral root initiated when reducing symplastic communication in the XPP. Supporting this hypothesis, increasing callose deposition by expressing ectopically PDCB1 or CALS3 in the XPP (in estradiol-treated J0121>>cals3m) increased LR density and reduced the spacing between initiated primordia (Fig. 6-7).

We propose that regulated intercellular connectivity plays a central role in LR development specifically by influencing the number and spatial organization of pericycle cells forming lateral roots. This adds a new facet to our understanding of LR organogenesis and patterning beyond the well-studied role of hormones. In identifying that regulation of symplastic connectivity, by callose turnover, is essential to LR patterning these data raise intriguing questions relating to the nature of crosstalk between hormone signaling and symplastic communication. PD connectivity might regulate the non-cell autonomous activity of auxin-inducible factors, such as Target of MONOPTEROS 7 (Schlereth et al., 2010). Interestingly, a role for MONOPTEROS/ARF5-dependent pathways in the control of cell

division and identity in the pericycle has previously been described (De Smet et al., 2010). Future work will address the intricacies of these mechanisms that are fundamental to the establishment of optimal root architecture and for general plant performance.

Experimental Procedures

Plant Material

Arabidopsis thaliana Columbia (Col-0) knockout lines were obtained for PdBG1 (SAIL_389_H11), PdBG2 (SALK_046127) and PdBG3 (SALK_14587) from NASC. We also obtained transposon insertional mutants (insertions in the same orientation of the gene) in Ler background from the CSHL (http://genetrap.cshl.edu/) and JIC SM collection for PdBG1 (GT_5_41639), PdBG2 (GT10161) and PdBG3 (ET82). The *pdbg1,2* double mutant, in Col and Ler background, was generated by crossing the single mutant lines. Primers for genotyping are in table S2.

Seeds were sterilized and germinated in long day conditions on plates containing MS medium. For estradiol induction, seedlings were germinated in MSO (MS without sucrose) and transferred after 6 days to MSO supplemented with 10 µM 17 β-estradiol. Lateral root phenotypes were evaluated at 24, 48 and 72h after treatment.

Molecular Biology and generation of transgenics

Transgenic seeds expressing p*GATA23*::GUS-nlsGFP, p*SHR*::SHR:GFP, p*SUC2*::mGFP6, p*AUX1*::AUX1:YFP, and p*DR5*::3xVENUS were requested (De Rybel et al., 2010; Brunoud et al., 2012; Benitez-Alfonso et al., 2009; Nakajima et al., 2001; Swarup et al., 2004). Construction of the p*35S*::mCherry-PDCB1 (PDCB1OE) has been described before (Simpson et al., 2009). In all cases expression of the constructs in mutant or over-expression background was achieved by crossing transgenic lines.

To obtain p*AUX1*-GFP, the promoter region of *AUX1* was amplified using primers cited in Table S2. Using multisite-Gateway technology, we inserted cytoplasmic mGFP6 (used to generate p*SUC2*::mGFP6) under the control of this promoter. pB7WG was used as destination vector.

N-terminal and GPI-anchor domains were predicted for PdBG1, PdBG2 and PdBG3 using DGPI and TargetP. Therefore the fluorescent tagged proteins were obtained by fusing in frame the structural proteins, the mCitrine and the GPI anchoring domains (using published protocols (Tian et al., 2004)). Primers designed for overlapping PCR are cited in table S2. The mCitrine-tagged proteins were subcloned in pDNR221 and then into the Gateway binary vector pB7WG2.0.

The inducible line J0121>>icals3m was obtained by introducing the p*6xUAS::*icals3m expressed in a modified version of pER8 (an estrogen-receptor based chemical-inducible system) in the enhancer trap line J0121 (www.plantsci.cam.ac.uk/Haseloff/) as described elsewhere (Vaten et al., 2011).

GUS staining and dye loading

Standard protocols were used for GUS assays (Simpson et al., 2009). Stained roots were mounted in chloral hydrate solution (1.3 g/mL chloral hydrate, 33% glycerol) and visualized in a Leica DM 6000.

To assess symplastic permeability, 10 day-old roots were exposed to 50 µg/ml carboxyfluorescein diacetate (CFDA, Sigma) for 5 and 30 min and thoroughly washed with water before microscopy. Differences in dye loading between PdBG1OE and wild-type were evident after 5 min staining.

Callose staining, immunolocalization and quantification

For callose immunolocalization, 6 day old seedlings were fixed in 4% paraformaldehyde, 0.01% Triton in PBS for 1hr at RT and mounted on glutaraldehyde-activated APTES (γ-aminopropyltriethoxysilane)-coated multiwell slides. Epidermal material was shaved off to aid penetration of antibodies. Samples were then air dried, treated with 2% Pectinase, 0.01% Pectolyase Y23 in PBS for 30 min at 37˚C, washed in PBS, blocked in 3%BSA/PBS and finally incubated in anti -callose (Biosupplies) diluted 1:400 in blocking solution overnight at 4˚C. After washing in PBS, anti-mouse alexa 488 (Invitrogen) diluted 1:200 in blocking solution, was applied for 2 hours at RT. Finally roots were washed in PBS, stained for 30min in 1µg/ml DAPI, and mounted in Vectashield.

Regular staining of callose was performed in leaves and root by vacuum infiltration with 0.1mg/mL aniline blue solution. To analyze wound-induced callose, leaves were pierced with tweezers and immediately infiltrated with aniline blue solution. For callose quantification, seedlings were fixed in MA (50% methanol and 10% acetic acid), treated with Propidium Iodide-Schiff reagent and stained with aniline blue 0.5mg/mL (Truernit et al., 2008). Confocal images of different roots were taken at the same resolution (pinhole) avoiding over-exposure. Regions of interest (ROI) of were drawn in comparable developmental areas containing LRP and/or immediately adjacent tissue and the mean gray value was determined using LAS AS Lite Software. At least three independent replicates were used to calculate each average and standard deviation using M. Excel package.

Microscopy

For counterstaining, roots were briefly exposed to 0.1µg/ml FM4-64 (Invitrogen) before microscopy. Confocal analysis was performed on a Leica SP5 or Zeiss LSM510 confocal microscopes using a 488nm excitation laser for GFP, m-Citrine and Alexa 488, the 405nm laser for aniline blue fluorochrome and DAPI and 561nm (DPSS) laser for mRFP and mCherry.

For anatomical, histological and reporter gene analyses 10 days old roots from vertically grown seedlings were used. Images were captured digitally with a Leica DM6000 equipped with Nomarski optics (DIC) and analyzed with the Image J software (http://rsbweb.nih.gov/ij).

Microprojectile Bombardment

Microprojectile bombardment assays were performed as described (Thomas et al., 2008). 4-6 week old expanded leaves of relevant Arabidopsis lines were bombarded with gold particles coated with pB7WG2.0.mRFP using a Bio-Rad Biolostic® PDS-1000/He Particle Delivery System. Bombardment sites were imaged 24h post-bombardment by confocal microscopy. Data was collected for a total of 97 bombardment sites for each genotype from at least 3 independent bombardment experiments,

each of which consisted of leaves from at least two individual plants. Statistical Poisson regression analysis was performed using GraphPad Prism version 5.04.

Statistical analysis of meristem size, lateral root density and emergence phenotypes

Cleared root preparations were characterized as described (Dubrovsky and Forde, 2012). We recorded the total number of primordia and emerged lateral roots (new meristems sticking out the main root) as well as total root length in 10 day old seedlings to calculated density (number of lateral root initiation events per mm of main root) and emergence (percentage of emerged lateral roots from the total number of lateral root initiation events). To investigate emergence phenotypes we synchronized lateral root initiation by applying a gravitropic stimulus (90^0 rotation of plates) to 3 days-old seedlings grown vertically on 0.5xMS plates (Peret et al., 2012) and counted the number of 'emerging' (stage VII) primordia, in the outer edge of the bend, 42 hours after gravi-stimulation. We measured root meristem size as the distance from the QC to the end of cell division. P value was calculated using two-tailed Student t-test.

Reference List

Aloni,R., Aloni,E., Langhans,M., and Ullrich,C.I. (2006). Role of cytokinin and auxin in shaping root architecture: regulating vascular differentiation, lateral root initiation, root apical dominance and root gravitropism. Ann. Bot. *97*, 883-893.

Bayer,E.M., Bottrill,A.R., Walshaw,J., Vigouroux,M., Naldrett,M.J., Thomas,C.L., and Maule,A.J. (2006). Arabidopsis cell wall proteome defined using multidimensional protein identification technology. Proteomics. *6*, 301-311.

Benitez-Alfonso,Y., Cilia,M., San,R.A., Thomas,C., Maule,A., Hearn,S., and Jackson,D. (2009). Control of Arabidopsis meristem development by thioredoxin-dependent regulation of intercellular transport. Proc. Natl. Acad. Sci. U. S. A *106*, 3615-3620.

Benitez-Alfonso,Y., Jackson,D., and Maule,A. (2010). Redox regulation of intercellular transport. Protoplasma *248*, 131-140.

Benkova,E. and Bielach,A. (2010). Lateral root organogenesis - from cell to organ. Curr. Opin. Plant Biol. *13*, 677-683.

Brunoud,G., Wells,D.M., Oliva,M., Larrieu,A., Mirabet,V., Burrow,A.H., Beeckman,T., Kepinski,S., Traas,J., Bennett,M.J., and Vernoux,T. (2012). A novel sensor to map auxin response and distribution at high spatio-temporal resolution. Nature *482*, 103-106.

Chen,X.Y., Liu,L., Lee,E., Han,X., Rim,Y., Chu,H., Kim,S.W., Sack,F., and Kim,J.Y. (2009). The Arabidopsis callose synthase gene GSL8 is required for cytokinesis and cell patterning. Plant Physiol *150*, 105-113.

De Rybel,B., Vassileva,V., Parizot,B., Demeulenaere,M., Grunewald,W., Audenaert,D., Van,C.J., Overvoorde,P., Jansen,L., Vanneste,S., Moller,B., Wilson,M., Holman,T., Van,I.G., Brunoud,G., Vuylsteke,M., Vernoux,T., De,V.L., Inze,D., Weijers,D., Bennett,M.J., and Beeckman,T. (2010). A novel aux/IAA28 signaling cascade activates GATA23-dependent specification of lateral root founder cell identity. Curr. Biol. *20*, 1697-1706.

De Smet,I., Lau,S., Voss,U., Vanneste,S., Benjamins,R., Rademacher,E.H., Schlereth,A., De,R.B., Vassileva,V., Grunewald,W., Naudts,M., Levesque,M.P., Ehrismann,J.S., Inze,D., Luschnig,C., Benfey,P.N., Weijers,D., Van Montagu,M.C., Bennett,M.J., Jurgens,G., and Beeckman,T. (2010). Bimodular auxin response controls organogenesis in Arabidopsis. Proc. Natl. Acad. Sci. U. S. A *107*, 2705-2710.

De Smet,I., Vanneste,S., Inze,D., and Beeckman,T. (2006). Lateral root initiation or the birth of a new meristem. Plant Mol. Biol. *60*, 871-887.

De Smet,I., Vassileva,V., De,R.B., Levesque,M.P., Grunewald,W., Van,D.D., Van,N.G., Naudts,M., Van,I.G., De,C.R., Wang,J.Y., Meuli,N., Vanneste,S., Friml,J., Hilson,P., Jurgens,G., Ingram,G.C., Inze,D., Benfey,P.N., and Beeckman,T. (2008). Receptor-like kinase ACR4 restricts formative cell divisions in the Arabidopsis root. Science *322*, 594-597.

Doxey,A.C., Yaish,M.W., Moffatt,B.A., Griffith,M., and McConkey,B.J. (2007). Functional divergence in the Arabidopsis beta-1,3-glucanase gene family inferred by phylogenetic reconstruction of expression states. Mol. Biol. Evol. *24*, 1045-1055.

Dubrovsky,J.G. and Forde,B.G. (2012). Quantitative Analysis of Lateral Root Development: Pitfalls and How to Avoid Them. Plant Cell *24*, 4-14.

Fernandez-Calvino,L., Faulkner,C., Walshaw,J., Saalbach,G., Bayer,E., Benitez-Alfonso,Y., and Maule,A. (2011). Arabidopsis plasmodesmal proteome. PLoS. One *6*, e18880.

Guseman,J.M., Lee,J.S., Bogenschutz,N.L., Peterson,K.M., Virata,R.E., Xie,B., Kanaoka,M.M., Hong,Z., and Torii,K.U. (2010). Dysregulation of cell-to-cell connectivity and stomatal patterning by loss-of-function mutation in Arabidopsis chorus (glucan synthase-like 8). Development *137*, 1731-1741.

Kim,J.Y., Yuan,Z., Cilia,M., Khalfan-Jagani,Z., and Jackson,D. (2002). Intercellular trafficking of a KNOTTED1 green fluorescent protein fusion in the leaf and shoot meristem of Arabidopsis. Proc. Natl. Acad. Sci. U. S. A *99*, 4103-4108.

Kim,J.Y., Yuan,Z., and Jackson,D. (2003). Developmental regulation and significance of KNOX protein trafficking in Arabidopsis. Development *130*, 4351-4362.

Lee,J.Y., Wang,X., Cui,W., Sager,R., Modla,S., Czymmek,K., Zybaliov,B., van,W.K., Zhang,C., Lu,H., and Lakshmanan,V. (2011). A plasmodesmata-localized protein mediates crosstalk between cell-to-cell communication and innate immunity in Arabidopsis. Plant Cell *23*, 3353-3373.

Levy,A., Erlanger,M., Rosenthal,M., and Epel,B.L. (2007a). A plasmodesmata-associated beta-1,3-glucanase in Arabidopsis. Plant J. *49*, 669-682.

Levy,A., Guenoune-Gelbart,D., and Epel,B.L. (2007b). beta-1,3-Glucanases: Plasmodesmal Gate Keepers for Intercellular Communication. Plant Signal. Behav. *2*, 404-407.

Lucas,M., Guedon,Y., Jay-Allemand,C., Godin,C., and Laplaze,L. (2008). An auxin transport-based model of root branching in Arabidopsis thaliana. PLoS. One *3*, e3673.

Malamy,J.E. and Benfey,P.N. (1997). Organization and cell differentiation in lateral roots of Arabidopsis thaliana. Development *124*, 33-44.

Marchant,A., Bhalerao,R., Casimiro,I., Eklof,J., Casero,P.J., Bennett,M., and Sandberg,G. (2002). AUX1 promotes lateral root formation by facilitating indole-3-acetic acid distribution between sink and source tissues in the Arabidopsis seedling. Plant Cell *14*, 589-597.

Marin,E., Jouannet,V., Herz,A., Lokerse,A.S., Weijers,D., Vaucheret,H., Nussaume,L., Crespi,M.D., and Maizel,A. (2010). miR390, Arabidopsis TAS3 tasiRNAs, and their AUXIN RESPONSE FACTOR targets define an autoregulatory network quantitatively regulating lateral root growth. Plant Cell *22*, 1104-1117.

Meng,L., Buchanan,B.B., Feldman,L.J., and Luan,S. (2012). CLE-like (CLEL) peptides control the pattern of root growth and lateral root development in Arabidopsis. Proc. Natl. Acad. Sci. U. S. A *109*, 1760-1765.

Moreira,S., Bishopp,A., Carvalho,H., and Campilho,A. (2013). AHP6 Inhibits Cytokinin Signaling to Regulate the Orientation of Pericycle Cell Division during Lateral Root Initiation. PLoS. One. *8*, e56370.

Moreno-Risueno,M.A., Van Norman,J.M., Moreno,A., Zhang,J., Ahnert,S.E., and Benfey,P.N. (2010). Oscillating gene expression determines competence for periodic Arabidopsis root branching. Science *329*, 1306-1311.

Muraro,D., Byrne,H., King,J., and Bennett,M. (2013). The role of auxin and cytokinin signalling in specifying the root architecture of Arabidopsis thaliana. J. Theor. Biol. *317*, 71-86.

Nakajima,K., Sena,G., Nawy,T., and Benfey,P.N. (2001). Intercellular movement of the putative transcription factor SHR in root patterning. Nature *413*, 307-311.

Oparka,K.J., Prior,D., and Wright,K.M. (1995). Symplastic communication between primary and developing lateral roots of *Arabidopsis thaliana*. J. Exp. Bot. *46*, 187-197.

Parizot,B., De,R.B., and Beeckman,T. (2010). VisuaLRTC: a new view on lateral root initiation by combining specific transcriptome data sets. Plant Physiol *153*, 34-40.

Parizot,B., Laplaze,L., Ricaud,L., Boucheron-Dubuisson,E., Bayle,V., Bonke,M., De,S., I, Poethig,S.R., Helariutta,Y., Haseloff,J., Chriqui,D., Beeckman,T., and Nussaume,L. (2008). Diarch symmetry of the vascular bundle in Arabidopsis root encompasses the pericycle and is reflected in distich lateral root initiation. Plant Physiol *146*, 140-148.

Peret,B., De,R.B., Casimiro,I., Benkova,E., Swarup,R., Laplaze,L., Beeckman,T., and Bennett,M.J. (2009). Arabidopsis lateral root development: an emerging story. Trends Plant Sci. *14*, 399-408.

Peret,B., Li,G., Zhao,J., Band,L.R., Voss,U., Postaire,O., Luu,D.T., Da,I.O., Casimiro,I., Lucas,M., Wells,D.M., Lazzerini,L., Nacry,P., King,J.R., Jensen,O.E., Schaffner,A.R., Maurel,C., and Bennett,M.J. (2012). Auxin regulates aquaporin function to facilitate lateral root emergence. Nat. Cell Biol. *14*, 991-998.

Rinne,P.L., Welling,A., Vahala,J., Ripel,L., Ruonala,R., Kangasjarvi,J., and van der,S.C. (2011). Chilling of dormant buds hyperinduces FLOWERING LOCUS T and recruits GA-inducible 1,3-beta-glucanases to reopen signal conduits and release dormancy in Populus. Plant Cell *23*, 130-146.

Schlereth,A., Moller,B., Liu,W., Kientz,M., Flipse,J., Rademacher,E.H., Schmid,M., Jurgens,G., and Weijers,D. (2010). MONOPTEROS controls embryonic root initiation by regulating a mobile transcription factor. Nature *464*, 913-916.

Simpson,C., Thomas,C., Findlay,K., Bayer,E., and Maule,A.J. (2009). An Arabidopsis GPI-anchor plasmodesmal neck protein with callose binding activity and potential to regulate cell-to-cell trafficking. Plant Cell *21*, 581-594.

Stadler,R., Wright,K.M., Lauterbach,C., Amon,G., Gahrtz,M., Feuerstein,A., Oparka,K.J., and Sauer,N. (2005). Expression of GFP-fusions in Arabidopsis companion cells reveals non-specific protein trafficking into sieve elements and identifies a novel post-phloem domain in roots. Plant J. *41*, 319-331.

Swarup,K., Benkova,E., Swarup,R., Casimiro,I., Peret,B., Yang,Y., Parry,G., Nielsen,E., De,S., I, Vanneste,S., Levesque,M.P., Carrier,D., James,N., Calvo,V., Ljung,K., Kramer,E., Roberts,R., Graham,N., Marillonnet,S., Patel,K., Jones,J.D., Taylor,C.G., Schachtman,D.P., May,S., Sandberg,G., Benfey,P., Friml,J., Kerr,I., Beeckman,T., Laplaze,L., and Bennett,M.J. (2008). The auxin influx carrier LAX3 promotes lateral root emergence. Nat. Cell Biol. *10*, 946-954.

Swarup,R., Kargul,J., Marchant,A., Zadik,D., Rahman,A., Mills,R., Yemm,A., May,S., Williams,L., Millner,P., Tsurumi,S., Moore,I., Napier,R., Kerr,I.D., and Bennett,M.J. (2004). Structure-function analysis of the presumptive Arabidopsis auxin permease AUX1. Plant Cell *16*, 3069-3083.

Thomas,C.L., Bayer,E.M., Ritzenthaler,C., Fernandez-Calvino,L., and Maule,A.J. (2008). Specific targeting of a plasmodesmal protein affecting cell-to-cell communication. PLoS. Biol. *6*, e7.

Tian,G.W., Mohanty,A., Chary,S.N., Li,S., Paap,B., Drakakaki,G., Kopec,C.D., Li,J., Ehrhardt,D., Jackson,D., Rhee,S.Y., Raikhel,N.V., and Citovsky,V. (2004). High-throughput fluorescent tagging of full-length Arabidopsis gene products in planta. Plant Physiol *135*, 25-38.

Traas,J. and Vernoux,T. (2010). Plant science. Oscillating roots. Science *329*, 1290-1291.

Truernit,E., Bauby,H., Dubreucq,B., Grandjean,O., Runions,J., Barthelemy,J., and Palauqui,J.C. (2008). High-resolution whole-mount imaging of three-dimensional tissue organization and gene expression enables the study of Phloem development and structure in Arabidopsis. Plant Cell *20*, 1494-1503.

Truernit,E. and Sauer,N. (1995). The promoter of the Arabidopsis thaliana SUC2 sucrose-H+ symporter gene directs expression of beta-glucuronidase to the phloem: evidence for phloem loading and unloading by SUC2. Planta *196*, 564-570.

Van Norman,J.M., Breakfield,N.W., and Benfey,P.N. (2011). Intercellular communication during plant development. Plant Cell *23*, 855-864.

Vanneste,S., De,R.B., Beemster,G.T., Ljung,K., De,S., I, Van,I.G., Naudts,M., Iida,R., Gruissem,W., Tasaka,M., Inze,D., Fukaki,H., and Beeckman,T. (2005). Cell cycle progression in the pericycle is not sufficient for SOLITARY ROOT/IAA14-mediated lateral root initiation in Arabidopsis thaliana. Plant Cell *17*, 3035-3050.

Vaten,A., Dettmer,J., Wu,S., Stierhof,Y.D., Miyashima,S., Yadav,S.R., Roberts,C.J., Campilho,A., Bulone,V., Lichtenberger,R., Lehesranta,S., Mahonen,A.P., Kim,J.Y., Jokitalo,E., Sauer,N., Scheres,B., Nakajima,K., Carlsbecker,A., Gallagher,K.L., and Helariutta,Y. (2011). Callose biosynthesis regulates symplastic trafficking during root development. Dev. Cell *21*, 1144-1155.

Xu,X.M. and Jackson,D. (2010). Lights at the end of the tunnel: new views of plasmodesmal structure and function. Curr. Opin. Plant Biol. *13*, 684-692.

Xu,X.M., Wang,J., Xuan,Z., Goldshmidt,A., Borrill,P.G., Hariharan,N., Kim,J.Y., and Jackson,D. (2011). Chaperonins facilitate KNOTTED1 cell-to-cell trafficking and stem cell function. Science *333*, 1141-1144.

Zavaliev,R., Ueki,S., Epel,B.L., and Citovsky,V. (2011). Biology of callose (beta-1,3-glucan) turnover at plasmodesmata. Protoplasma *248*, 117-130.

Acknowledgments: We thank T. Beeckman, M.J. Bennett for kindly provided the GATA23 and the DR5 reporter lines. SHR and AUX1 translational fusion lines were obtained from P. Benfey and C. Kuhlemeier respectively. We acknowledge the contribution of C. Burt in statistical analysis, K.D.

O'Neill and J. Barnes as technical support. The John Innes Centre is grant-aided by the Biotechnology and Biological Science Research. The authors declare no conflicts of interest.

Figure Legends:

Fig. 1 Symplastic domains form during lateral root development. (**A**) Cartoon showing root developmental regions, LR stages and tissue organization (qc: quiescent center; Ep:epidermis; C:Cortex, E:endodermis and P:pericycle) as referred to in the text. Free GFP expression in p*SUC2*-GFP (**B-G**) and p*AUX1*-GFP (**H-M**) transgenic roots (10 days old). Movement of GFP from the phloem (p*SUC2*-GFP) and from the pericycle (p*AUX1*-GFP) is observed into endodermal (E), cortical (C) and epidermal (Ep) cell layers in (**B, H**). GFP diffusion is gradually restricted as primordia develop (**C-F, I-L**; position of LRP and approximate stage in brackets are indicated). GFP unloading is normal in emerged lateral roots (**G, M**). FM4-64 (red) was used as counterstain. Stages were assigned according to bright-field images (Fig. S1) and the description provided in the graphical abstract. Scale bars: 20µm.

Fig. 2 Callose deposition is regulated during lateral root development and is increased in *pdbg1,2*. Immuno-fluorescent detection of callose (green) in the basal meristem (**A**), stage I-II (**B**), stage III (**C**), IV-V (**D, E**), stage VII (**F**) and emerged (**G**) primordia. Immuno-localization of callose in non-lateral root (**H**) and lateral root (**I** and inset) regions of *pdbg1,2* seedlings. Nuclei were stained with DAPI (blue) and bright-field images were superimposed. Black arrows indicate PD-associated callose. Cell plate or sieve plate associated callose, primordium (LRP), cortex (C), endodermis (E), XPP and stele are also marked in **A-B** and **I.** Note the increase in callose deposited in the stele of *pdbg1,2* (**H, I** and inset) in comparison to equivalent regions in wild-type (**A, F**). See also Fig. S2. Scale bars: 10 µm.

Fig. 3. PdBG1 is a callose degrading enzyme expressed in PDs of early stage lateral root primordia. (**A-F**) *PdBG1* expression as revealed by GUS staining of transgenics expressing p*PdBG1*-GUS. Expression is higher in potential lateral root founder cells and stage III LRP (black arrows). Small insets in **A-B** indicate the region imaged (square) using as reference the root tip. See also Figure S3. PdBG1-mCit (mCitrine is fused in frame to the structural protein at position 452, green, **G, L**), callose deposits revealed by aniline blue staining (false colored in white in **H**) and mCherry-PDCB1 (red, **M**) co-localized at PDs in transgenic leaves (arrows in **I** and **N**). Localization at PDs is also found in roots (**J-K**; FM4-64 stained cell periphery in red). Wound-induced callose (W indicates initial wounding site) is reduced in PdBG1OE (**P**) in comparison to wild-type (**O**). Scale bars: 20 µm.

Fig. 4. Symplastic transport is regulated by PdBG1 and PdBG2. (**A-C**) GFP accumulation in the early LR forming zone (before any visible primordia) in *pdbg1,2* and wild-type siblings expressing p*SUC2*-GFP. GFP, primarily expressed in the phloem (Ph), moves (*) to the endodermis (E) and cortex (C) in wild-type roots (**A, C**). Symplastic movement is blocked in *pdbg1,2* roots (**B** and **C** lower panel). (**D,E**) SHR-GFP expression and mobility (arrowed) in wild-type and *pdbg1,2* lateral roots. FM4-64 (red) was used as a counterstain. (**F**) Biolistic experiments using mRFP as symplastic probe. Data was collected in three experimental replicas for a total of 97 bombardment sites per genotype. The graph represents the number of sites that showed movement away from the bombardment target cell to 0, 0-10, 11-30 and >30 cells. P <0.001 calculated by Poisson regression of the data. (**G-I)** Dye transport after exposure of wild-type (**G**) and PdBG1OE (**H,I**) roots to CFDA. Notice dye loading into PdBG1OE primordia (**H,I**). Differences in callose deposition are shown in Fig. S4. Scale bars: 20 µm.

Fig. 5. Mutations in PdBG1 and PdBG2 affect lateral root density by altering the spacing between primordia. (**A**) Lateral root density was calculated for 6 day old Col-0, *pdbg1*, *pdbg2*, and *pdbg1,2* roots. Error bars represent standard deviation (***, P<0.001). Fig. S5 shows the results with mutants

in Ler. (**B**) Examples of clustered and fused lateral roots found in *pdbg1,2*. Mutants showed extended regions of GATA23 (**D**) and DR5 (**F**) expression in comparison to wild-type siblings (**C, E**) consistent with the formation of clustered primordia (LRP). Distance between pre-branching sites (p) is distorted in the mutant (compare **E** and **F**). Roots were stained with FM4-64 (red). Scale bars: 20 µm.

Fig. 6. Callose deposition regulates the spacing between lateral root initiation sites. (**A**) Lateral root density in PdBG1OE and PDCB1OE roots (**, P<0.01; ***, P<0.001). GATA23 expression (green nuclei) in wild-type (**B**), PdBG1OE (**C,F**) and in PDCB1OE roots (**D,E**). In comparison to wild-type (**B**), overexpression of PdBG1 led to a significant increase in the distance between primordia (**C,F**). Conversely, primordia appear clustered in PDCB1OE (**D,E**). Wild-type roots were stained with FM4-64 (red) in **B**. Cell-walls fluoresce in green in (**C,F**) due to PdBG1-mCit expression at PD and in red in (**D,E**) due to mCherry-PDCB1. See also emergence phenotype in Fig. S6. Scale bars (**B-C, F**): 40 µm, (**D-E**): 20 µm.

Fig. 7. Altered lateral root distribution is a primary effect of induced callose deposition in the xylem-pole pericycle (XPP). (**A**) shows that the pattern of GFP expression in root tissues of the GAL4-GFP enhancer trap line J0121 is associated with mature XPP. Aniline blue staining revealed increased callose deposition after 24h estradiol treatment of roots expressing cals3m under an estradiol-inducible UAS promoter in the J0121 background (J0121>>cals3m) in comparison to non-induced control siblings (**B-C,** bright-field superimposed image is also shown for **C**). (**D**) Lateral root density in control (J0121 and untreated J0121>>cals3m) and estradiol-treated roots calculated 72 hpi (hours post-induction). LR primordia (arrows) are marked by GUS activity in control (**E** panels) and induced (48hpi) J0121>>cals3m (**F** panels) transgenics expressing p*GATA23*-GUS. Notice the neighboring primordia in **F** panels. Scale bars: 20 µm.

Figure 1

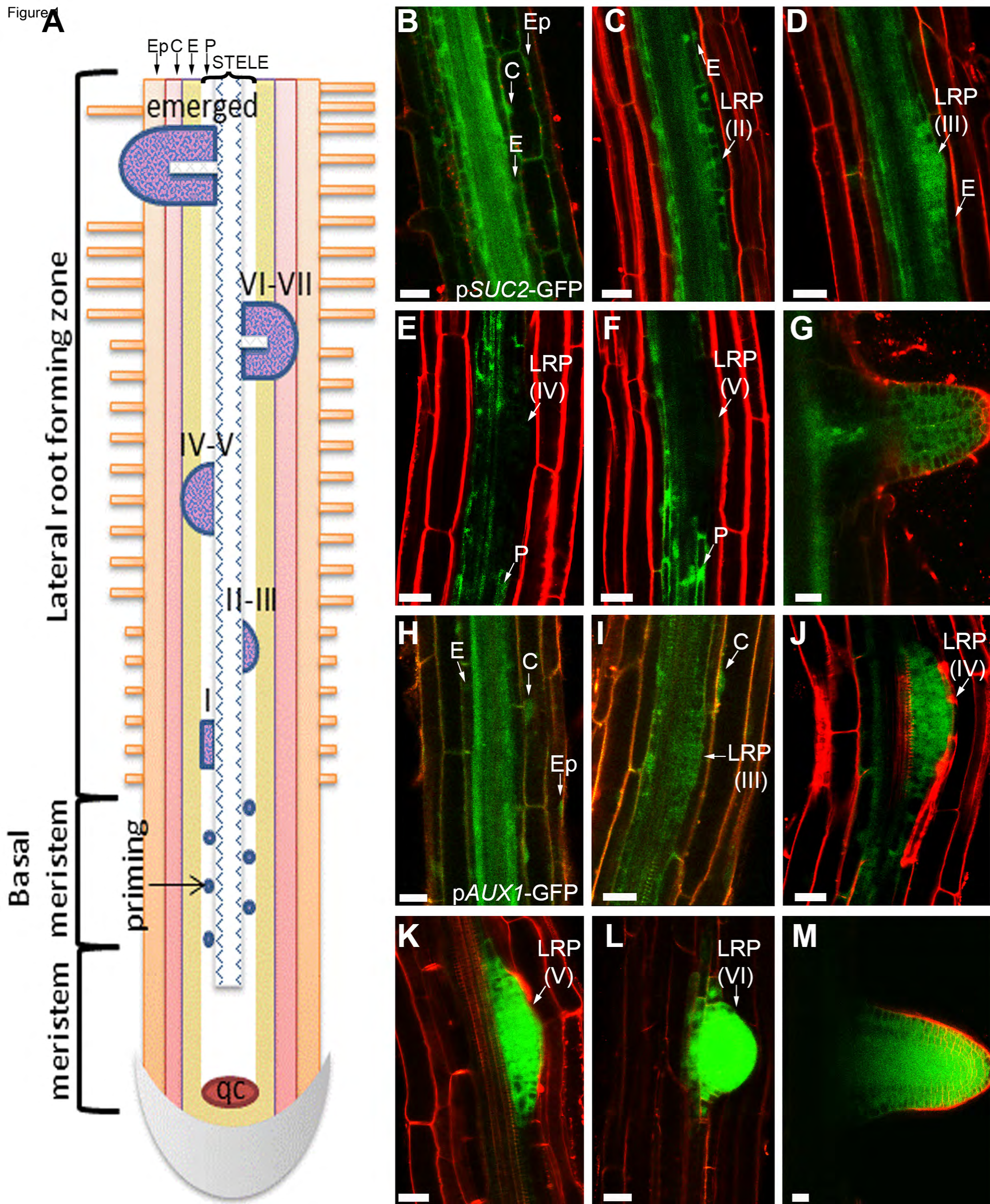
A
Ep C E P
STELE
emerged
VI-VII
IV-V
II-III
I
priming
Lateral root forming zone
Basal meristem
meristem
qc
B
Ep
C
E
pSUC2-GFP
C
E
LRP (II)
D
LRP (III)
E
E
LRP (IV)
P
F
LRP (V)
P
G
H
E
C
Ep
pAUX1-GFP
I
C
LRP (III)
J
LRP (IV)
K
LRP (V)
L
LRP (VI)
M

Figure 2

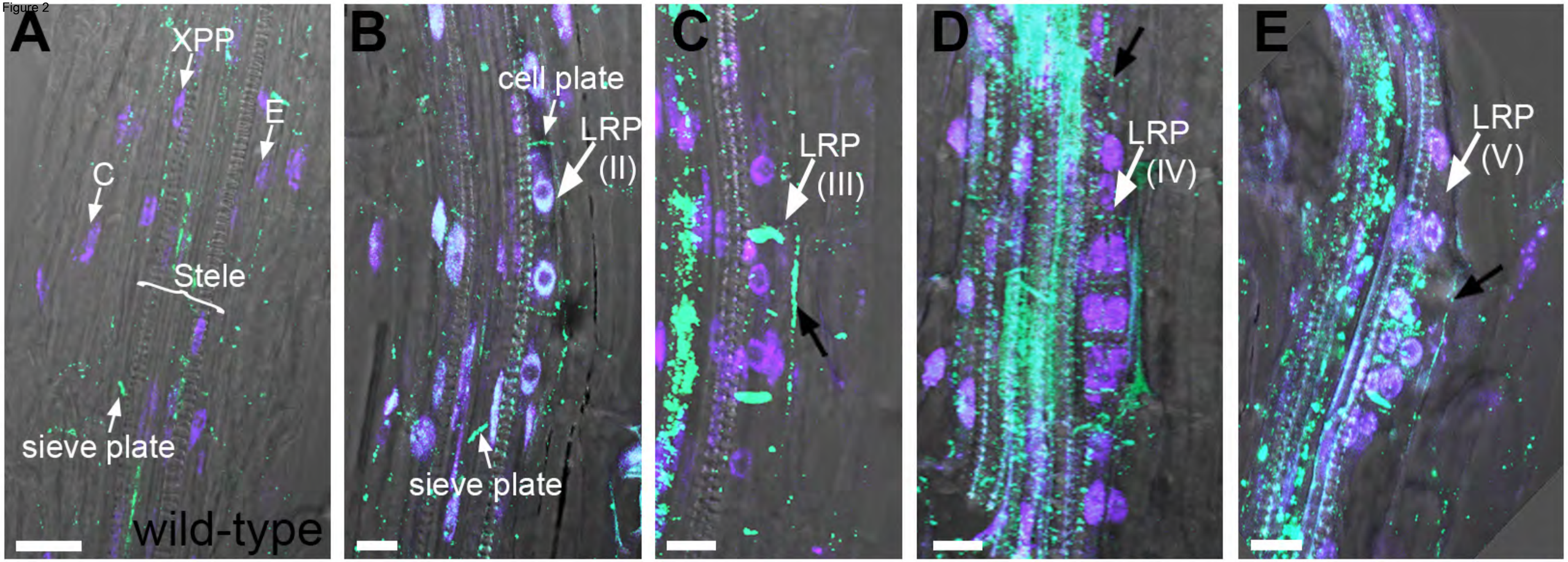
A
XPP
E
C
Stele
sieve plate
wild-type
B
cell plate
LRP
(II)
sieve plate
C
LRP
(III)
D
LRP
(IV)
E
LRP
(V)
F
LRP
(VII)
G
H
Stele
pdbg1,2
I
LRP
XPP
XPP
E
C

Figure 3

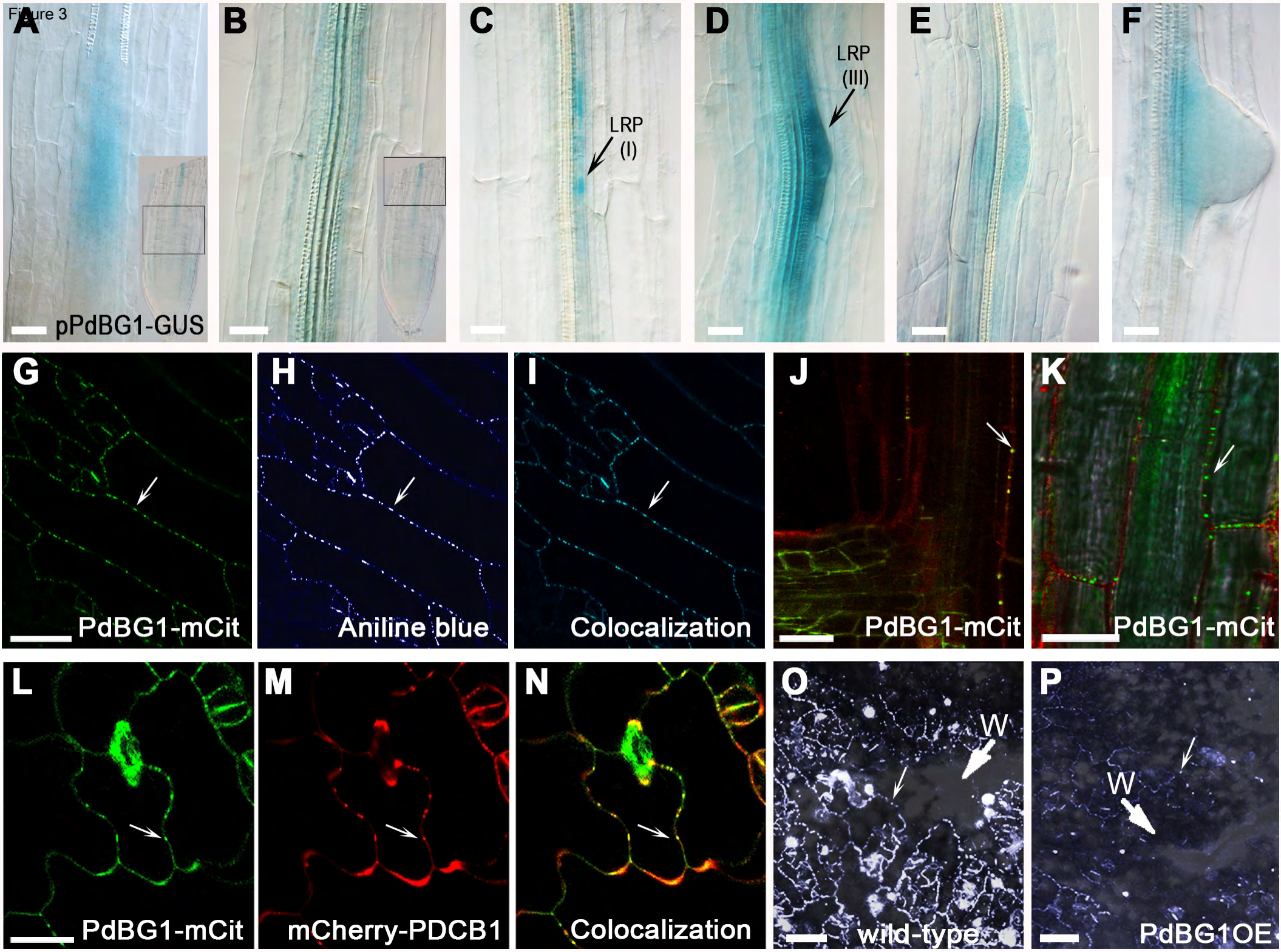
A
pPdBG1-GUS
B
C
LRP
(I)
D
LRP
(III)
E
F
G
PdBG1-mCit
H
Aniline blue
I
Colocalization
J
PdBG1-mCit
K
PdBG1-mCit
L
PdBG1-mCit
M
mCherry-PDCB1
N
Colocalization
O
W
wild-type
P
W
PdBG1OE

Fig 4

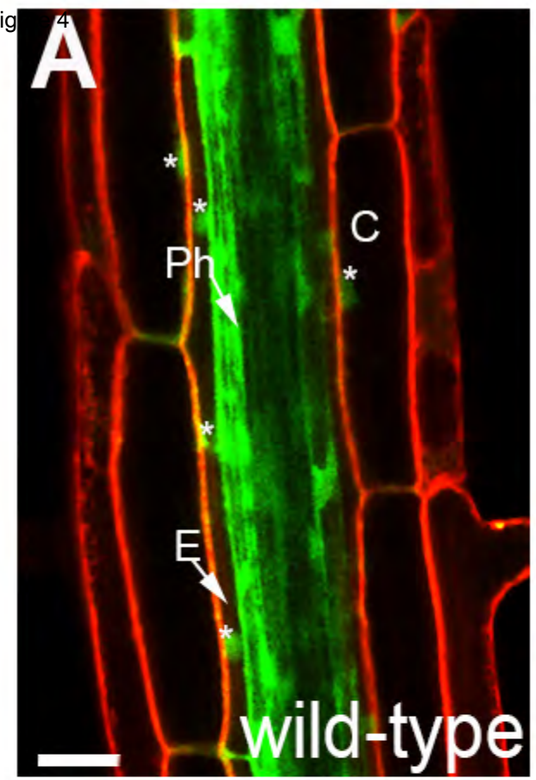
A
Ph
C
E
wild-type

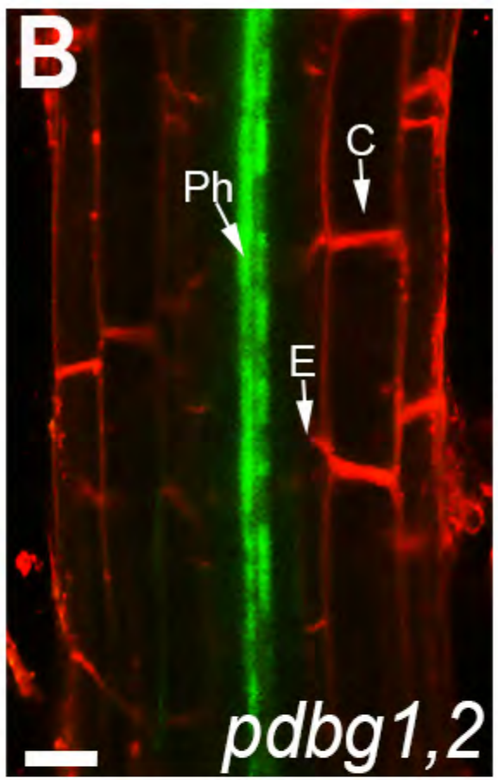
B
Ph
C
E
pdbg1,2

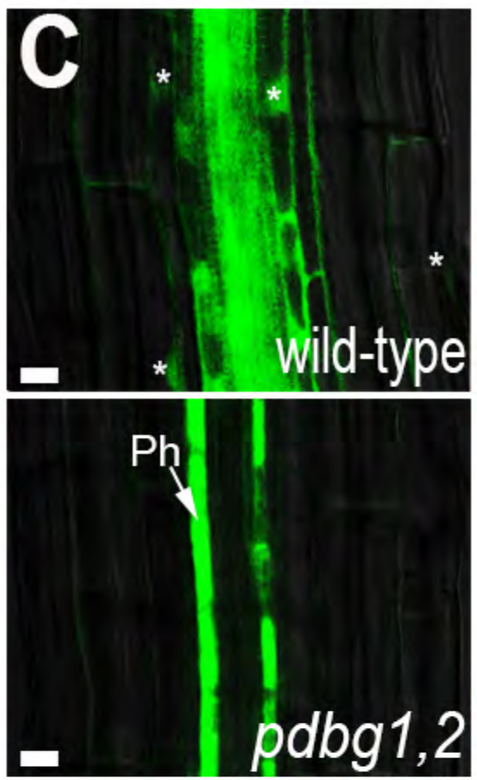
C
wild-type
Ph
pdbg1,2

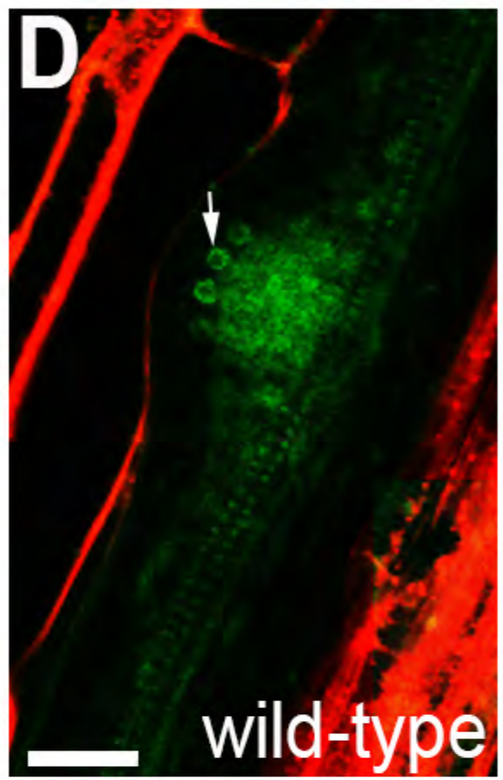
D
wild-type

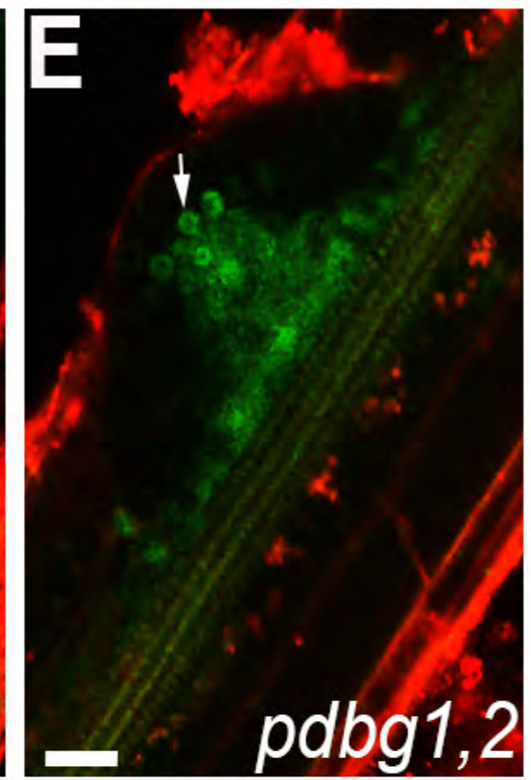
E
pdbg1,2

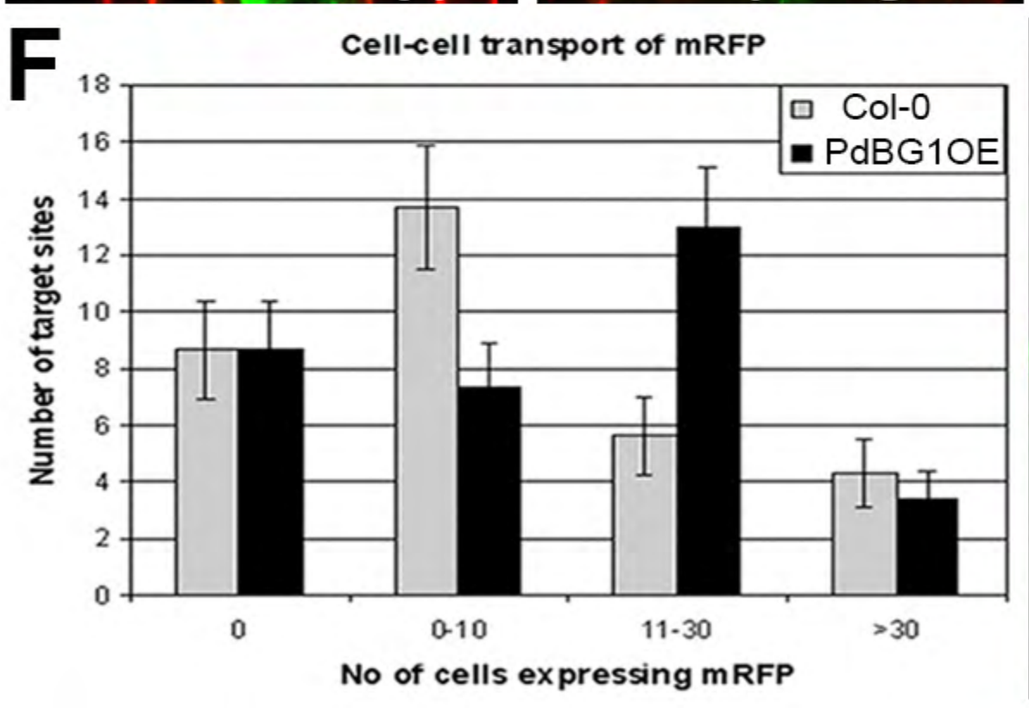
F
Cell-cell transport of mRFP
Col-0
PdBG1OE
Number of target sites
18
16
14
12
10
8
6
4
2
0
0
0-10
11-30
>30
No of cells expressing mRFP

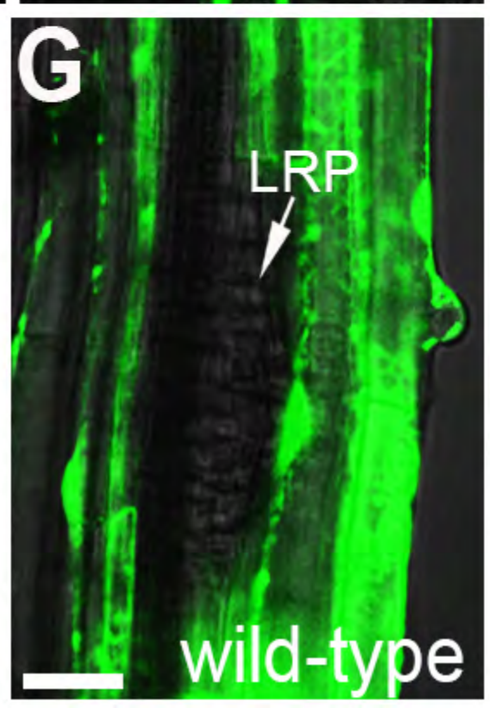
G
LRP
wild-type

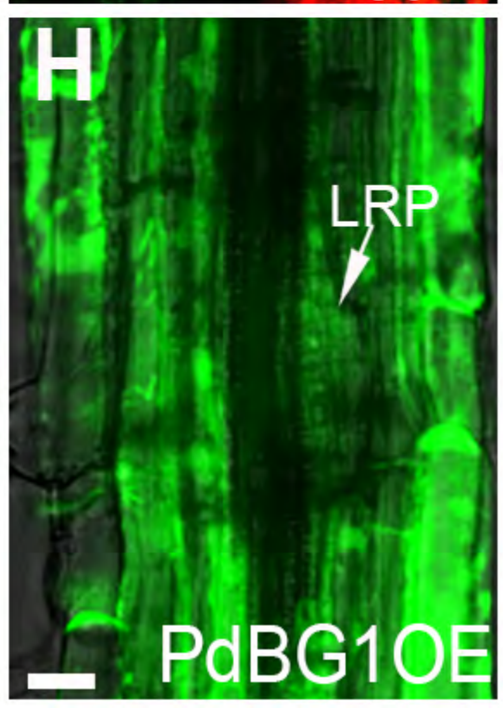
H
LRP
PdBG1OE

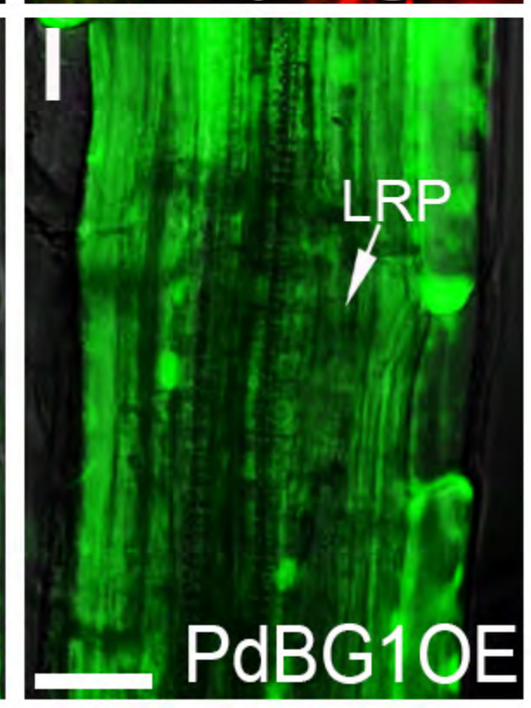
I
LRP
PdBG1OE

Figure 5

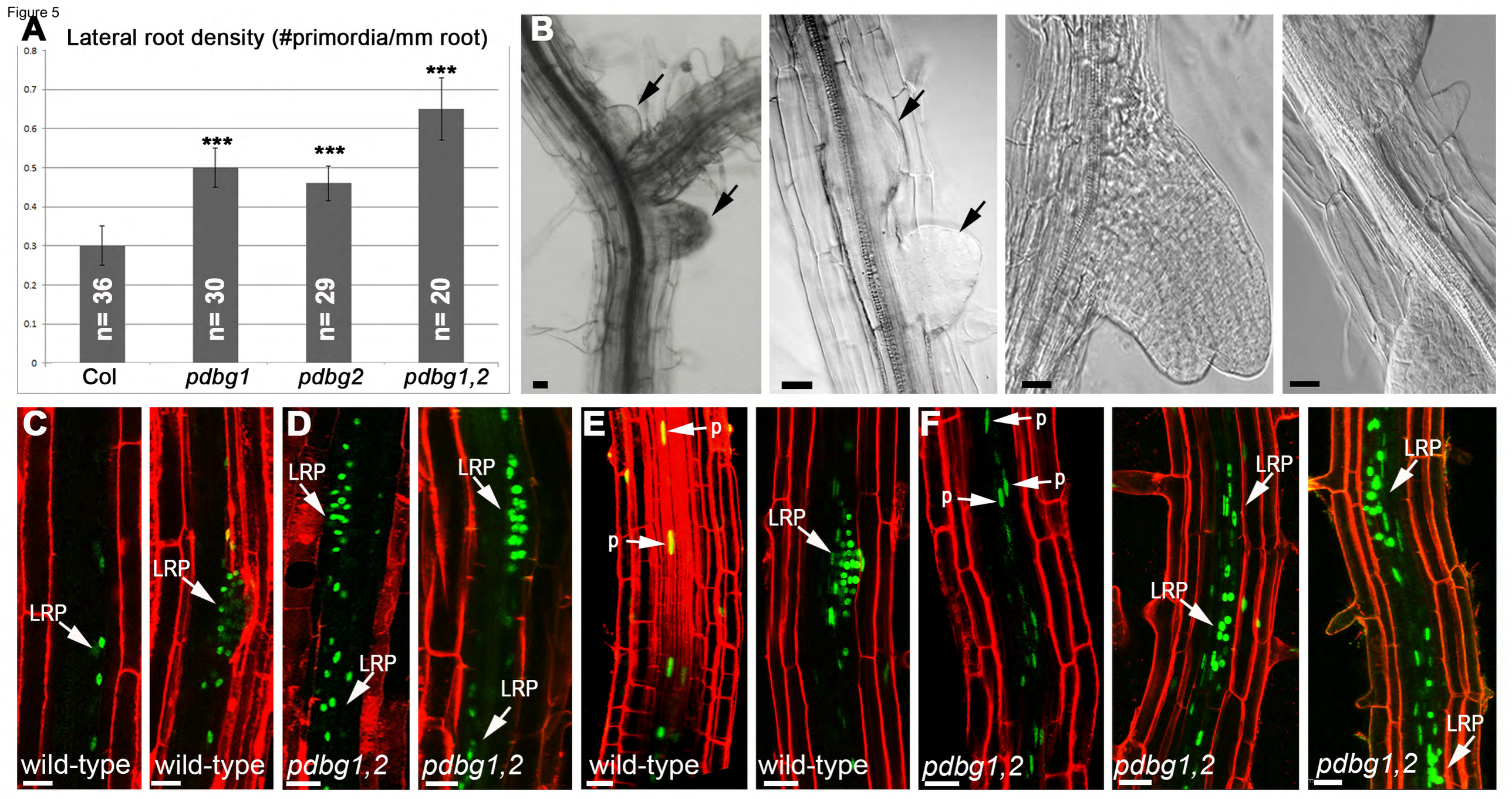
A
Lateral root density (#primordia/mm root)
0.8
0.7
0.6
0.5
0.4
0.3
0.2
0.1
0
***
***
***
n= 36
n= 30
n= 29
n= 20
Col
pdbg1
pdbg2
pdbg1,2
B
C
LRP
LRP
wild-type
wild-type
D
LRP
LRP
pdbg1,2
pdbg1,2
E
p
p
wild-type
LRP
wild-type
F
p
p
p
pdbg1,2
LRP
LRP
pdbg1,2
LRP
LRP
pdbg1,2

Figure 6

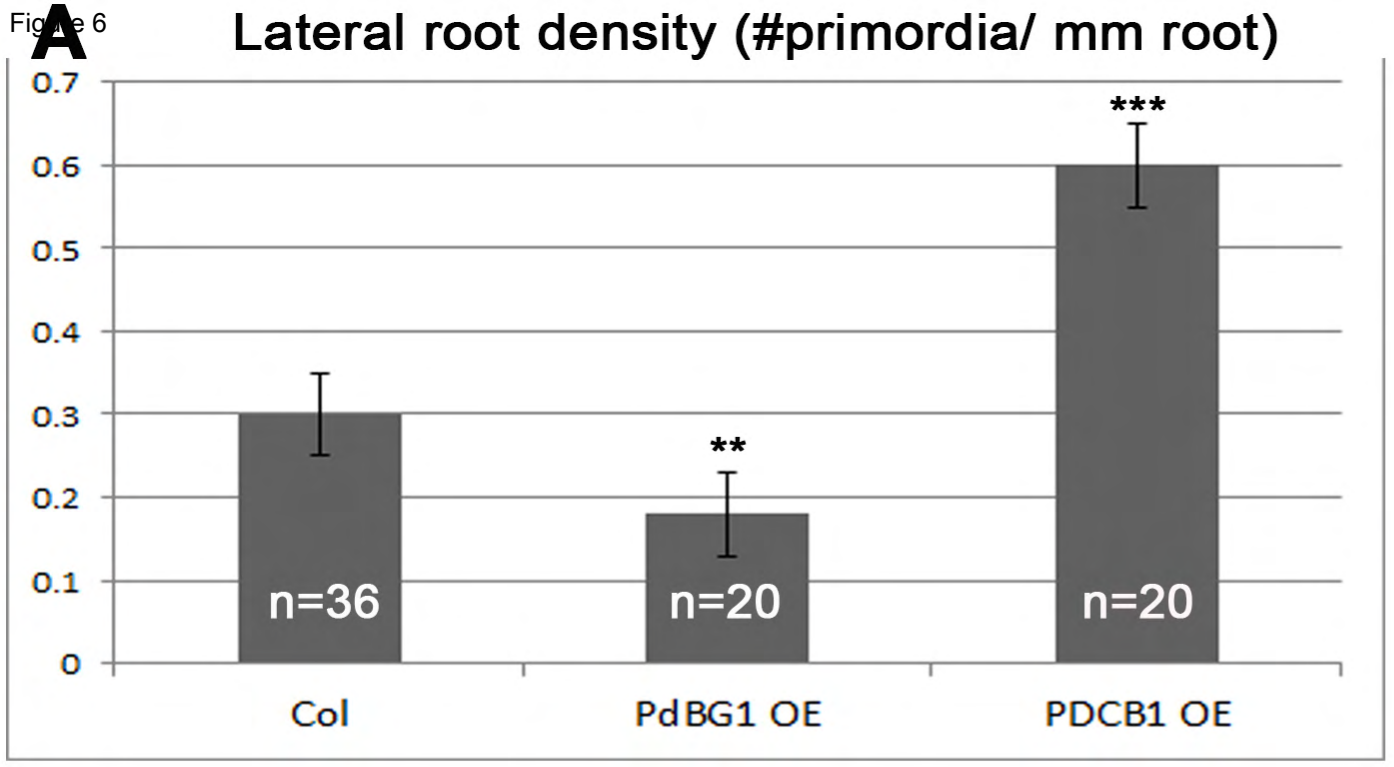
A
Lateral root density (#primordia/ mm root)
0.7
0.6
0.5
0.4
0.3
0.2
0.1
0
n=36
n=20
n=20
**
***
Col
PdBG1 OE
PDCB1 OE

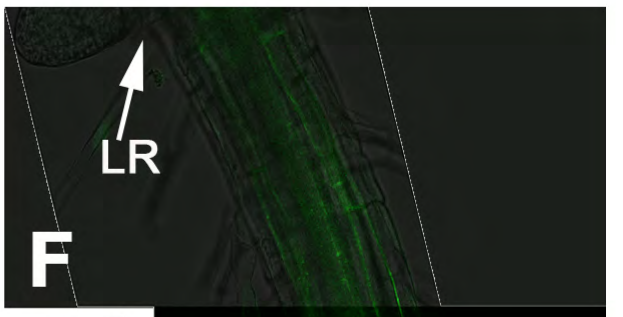
LR
F

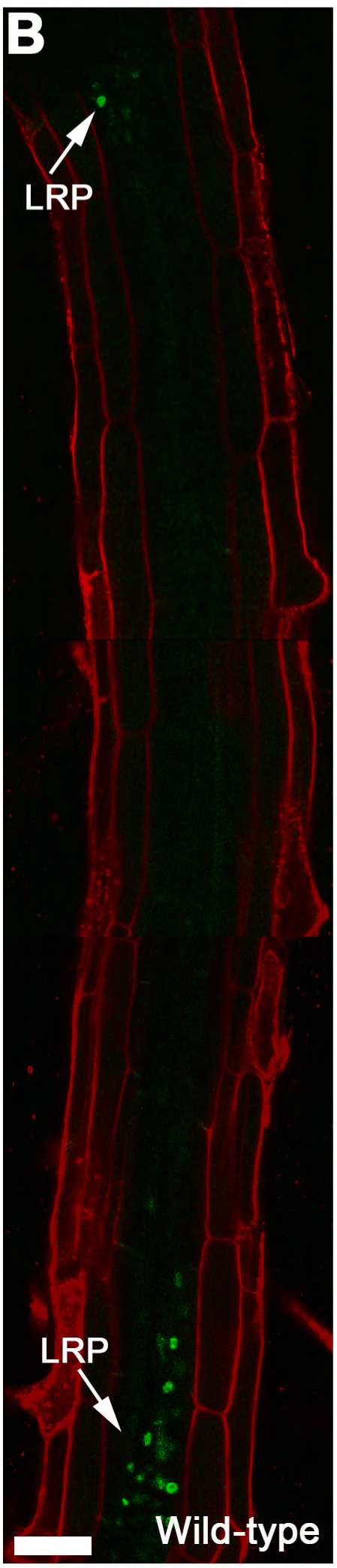
B
LRP
LRP
Wild-type

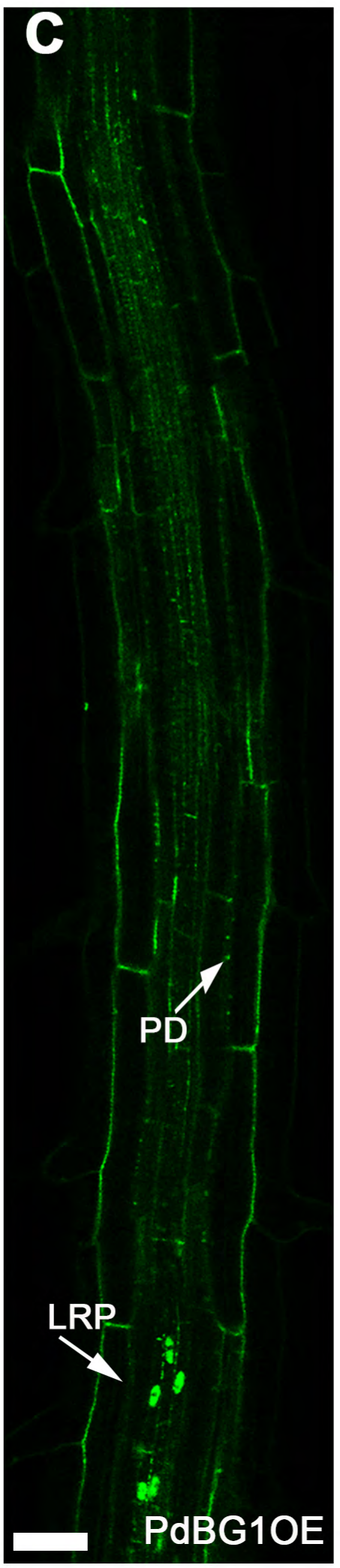
C
LRP
PD
LRP
PdBG1OE

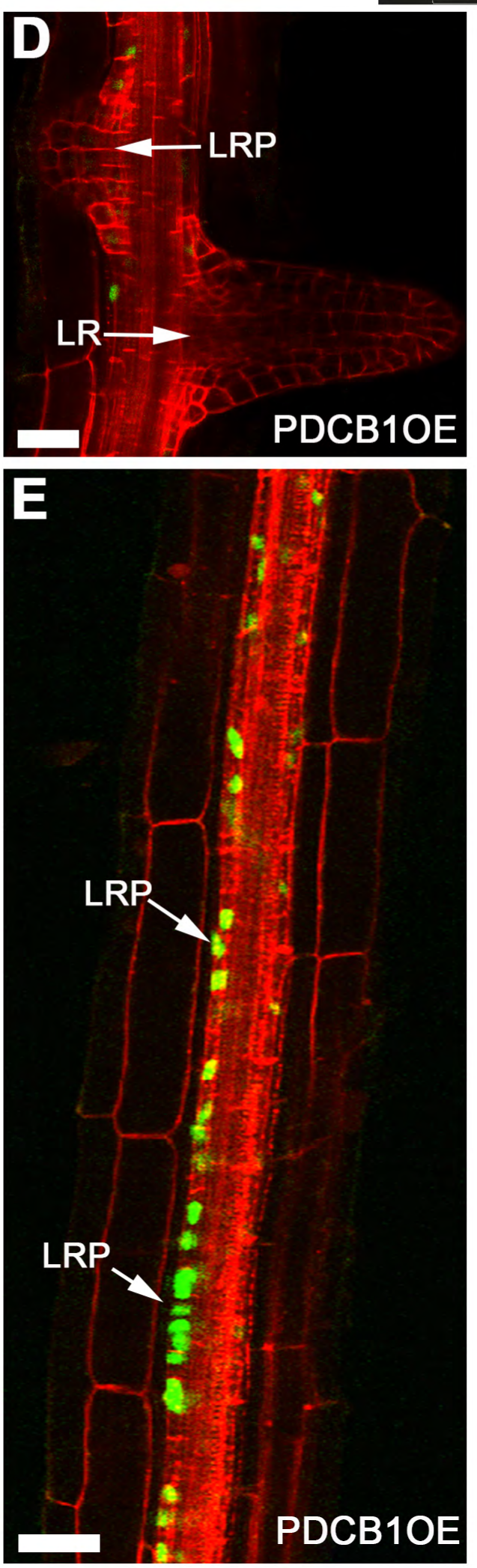
D
LRP
LR
PDCB1OE
E
LRP
LRP
PDCB1OE

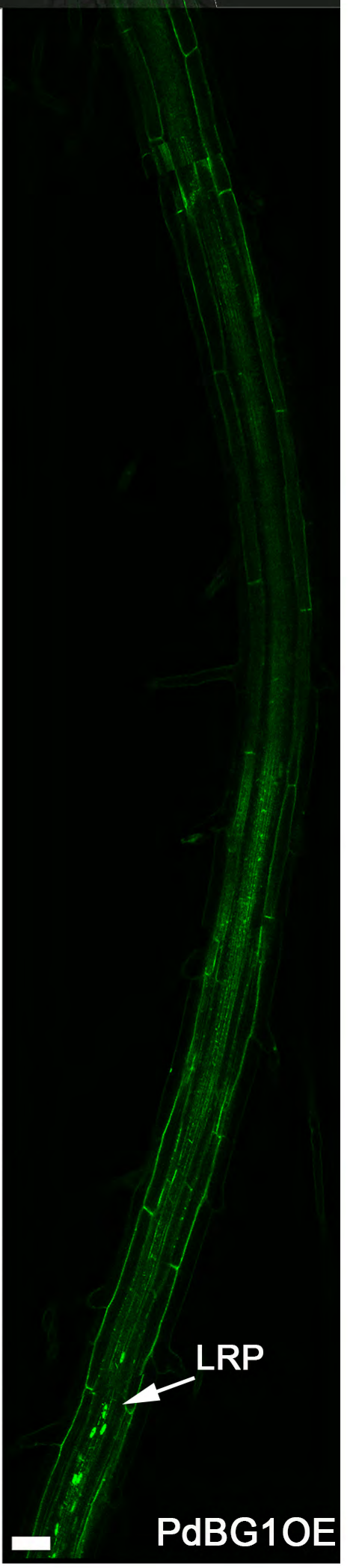
LRP
PdBG1OE

Figure 7

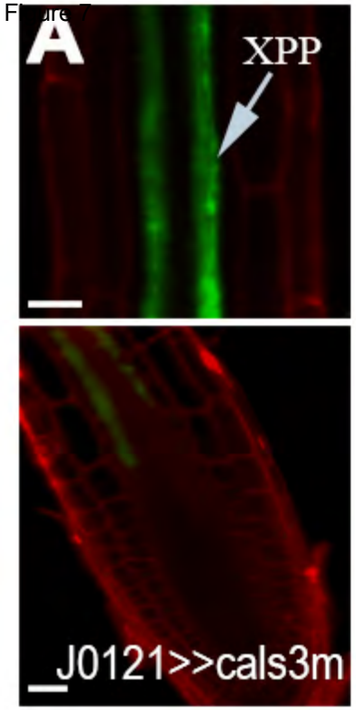
A
XPP
J0121>>cals3m

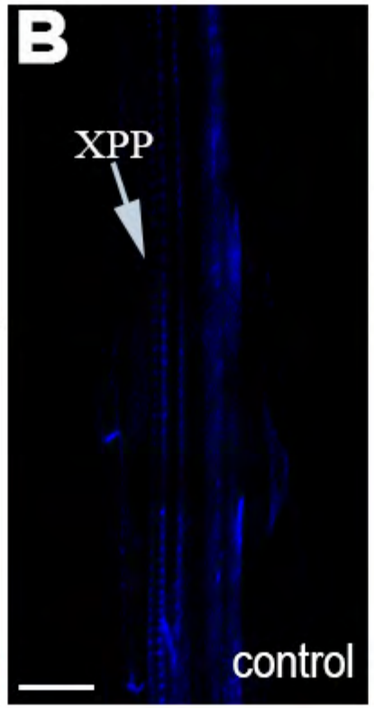
B
XPP
control

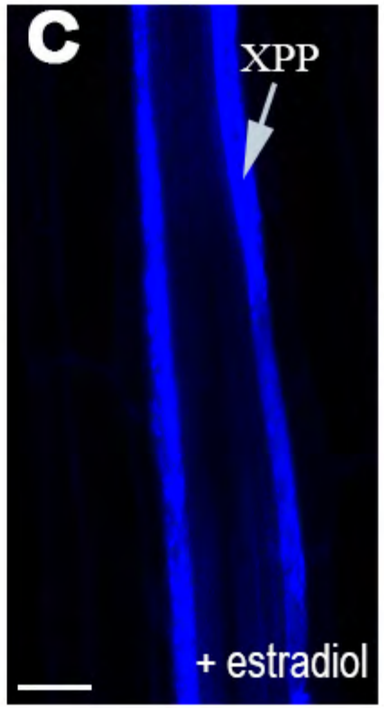
C
XPP
+ estradiol

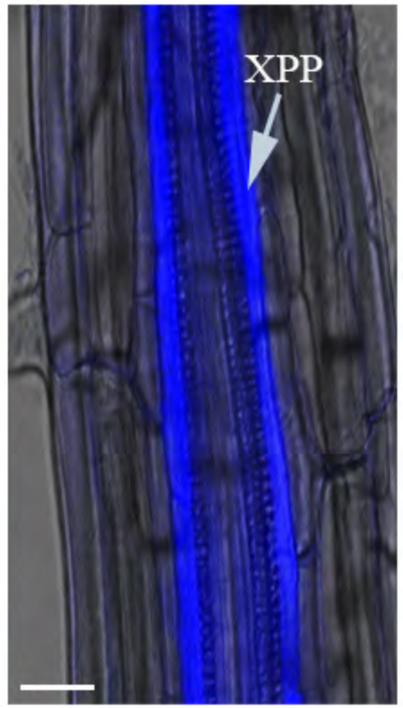
XPP

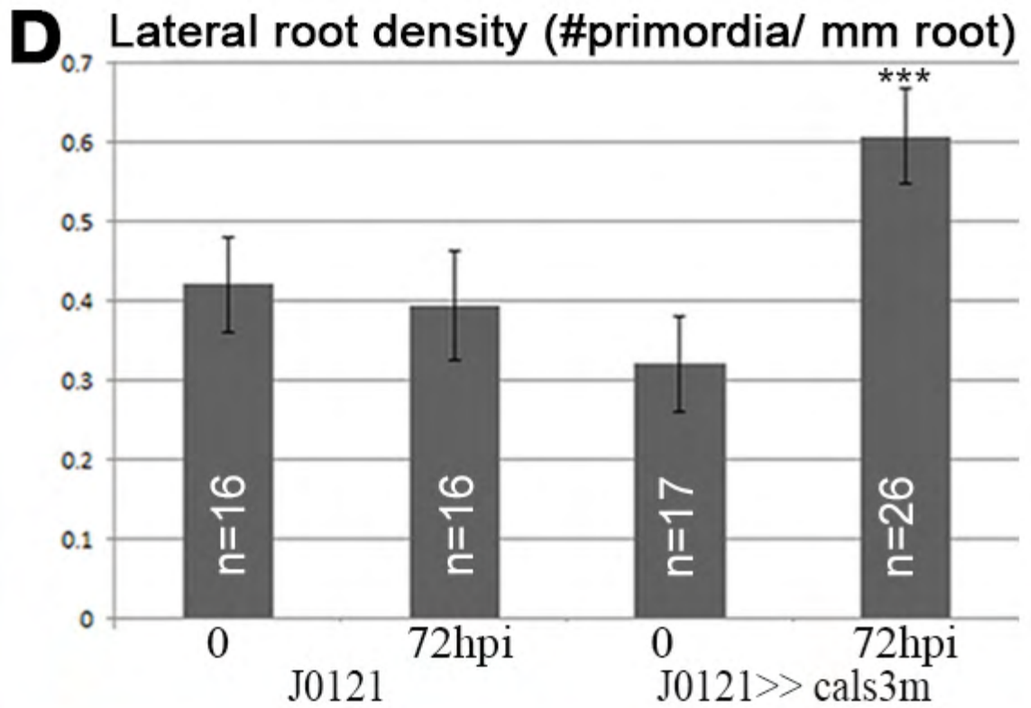
D
Lateral root density (#primordia/ mm root)
0.7
0.6
0.5
0.4
0.3
0.2
0.1
0
***
n=16
n=16
n=17
n=26
0
72hpi
0
72hpi
J0121
J0121>> cals3m


E
LRP
control

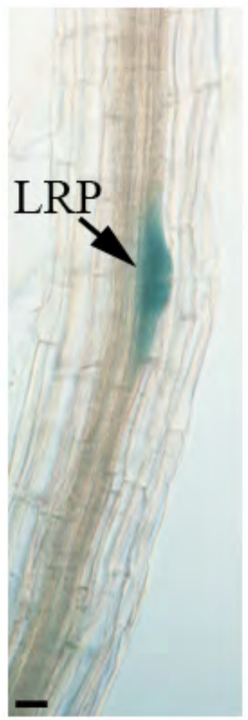
LRP


LRP

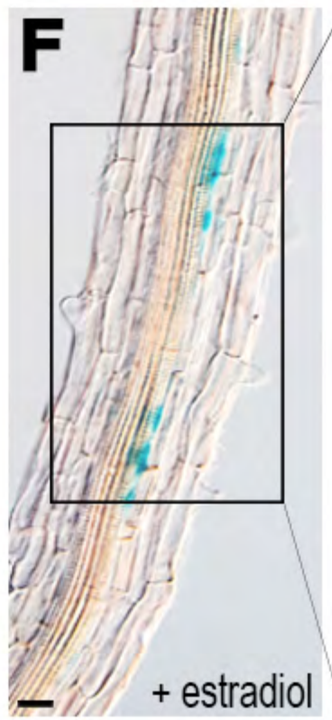
F
+ estradiol


LRP
LRP

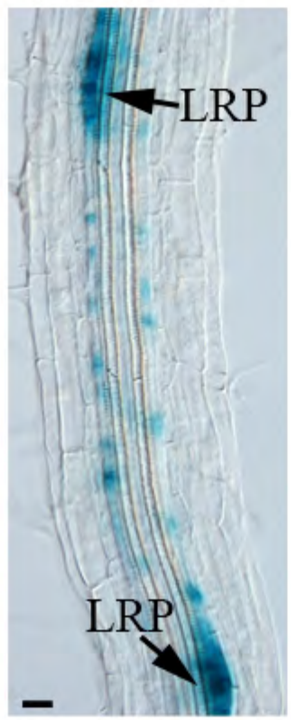
LRP
LRP


LRP
LRP

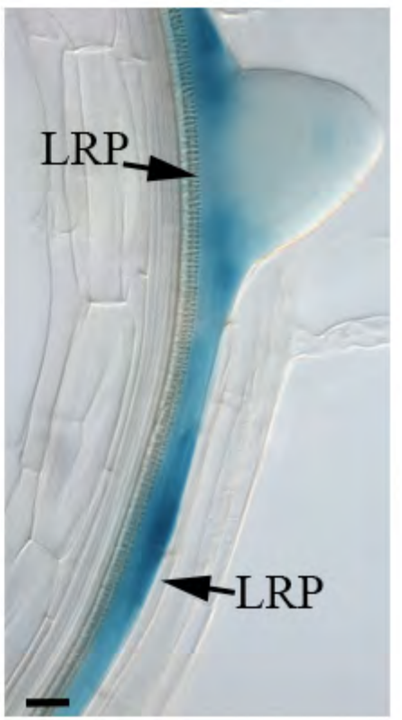
LRP
LRP

Fig S1, Related to Fig 1. It contains pictures in the bright-field channel for panels B-M in Fig.1 and expression of AUX1 (yellow) in the basal meristem and lateral root forming zone.

Fig S2, Related to Fig 2. Regulation of callose during lateral root development as revealed by aniline blue staining and quantified using fluorescence intensity.

Fig S3, Related to Fig 3. Expression and localization of PdBG1, 2 and 3.

Fig S4, Related to Fig 4. Staining and quantification of callose in LRPs of wild-type, *pdbg1,2* and PdBG1OE.

Fig S5, Related to Fig 5. Developmental phenotypes in *pdbg1,2* mutant and PdBG1 over-expression line.

Fig S6, Related to Fig 6. Lateral root emergence in mutant and over-expression lines.

Table S1, Related to Fig 3. Gene expression analysis of callose metabolic enzymes identified in the proteome of purified PD-enriched cell walls.

Table S2, Related to Experimental Procedures. Primers used for PCR amplification in this study.

Legend for Supplemental Figures and Tables

Fig S1, Related to Fig 1. (**A-L**) Pictures in the bright-field channel are shown for panels B-M in Fig.1 (lateral root primordium (LRP) indicated with a black arrow). (**M-S**) Expression of AUX1 (yellow) in the basal meristem and lateral root forming zone as revealed by confocal imaging of transgenic roots expressing AUX1-YFP under the native promoter. Notice that AUX1 expression is observed in the pericycle (and vascular tissue) of the basal meristem (before any evident LRP is formed) but this pattern changes during LR differentiation (lateral root forming zone) and expression is restricted to stage I-VII LRP. Once emergence occurs, expression in the new lateral root resembles the primary meristem (**S**). Scale bars: 20µm.

Fig S2, Related to Fig 2. Regulation of callose during lateral root development. (**A-E**) Aniline blue staining of callose (white, arrowed), in 10 day old roots, is very strong in stage III-V primordia (**B-C**) in comparison to non-LR regions (**A**) and emerged LR (**E**). Super-imposed bright-field channel is shown for **A-C** in (**A'-C'**). Scale bars: 20µm. Quantification, using fluorescence intensity, reflects these results (**F**). The mean gray value in the cell-wall bordering the primordium was corrected by subtracting the background fluorescence contained in the same area in the wall opposite the primordium. Results were averaged for three independent replicates per lateral root stage. Error bars represent standard deviation. Asterisks represent statistical significance: (**, P<0.01; ***, P<0.001).

Fig S3, Related to Fig 3. Expression and localization of PdBGs. (**A-E**) show *PdBG1* expression as revealed by GUS staining of the genetrap line GT_5_41639 (*pdbg1-GT*). Panel **F** shows expression in lateral root of PdBG1-mCit driven by the native promoter. Confocal images show mCitrine fluorescence (green, **G, J**) and aniline blue stained-callose (white, **H, K**) that co-localize (**I, L**) in transgenic leaves expressing PdBG2-mCit (**G-I**) and PdBG3-mCit (**J-L**). (**M-R**) *PdBG2* expression in lateral roots is revealed by GUS staining of the genetrap line GT10161 (*pdbg2-GT*). Notice endodermal expression in **M**. Scale bar: 20 µm.

Fig S4, Related to Fig 4. Aniline blue staining of callose (blue) in LRPs of wild-type (**A, C**), *pdbg1,2* (**B, D**) and PdBG1OE (**E**) (10 day old seedlings). Roots were fixed and counterstained with propidium iodide (red). Note the increase in callose deposited in *pdbg1,2* roots (arrowed). (**F**) Graphical representation of average fluorescent intensity (mean gray values) in the lateral root region relative to Col-0. Error bars are standard deviation. Scale bar: 20 µm. Labels stand for E: endodermis, C:cortex, Ep: epidermis.

Fig S5, Related to Fig 5. Developmental phenotypes in mutant and over-expression lines. (**A**) Lateral root density in single *pdbg1-GT* (GT_5_41639), *pdbg2-GT* (GT10161) and double *pdbg1,2-GT* in the Ler background. Error bars represent standard deviation. Asterisks represent statistical significance: (**, P<0.01; ***, P<0.001). (**B**) Wild-type, PdBG1OE and *pdbg1,2* seedlings 10 days post-germination in 0.5xMS medium. (**C**) No significant difference was observed upon measurement of meristem size in Col, *pdbg1,2* and PdBG1OE roots. Immuno-localization of callose (green) in the root meristem of wild-type (**D**) and *pdbg1,2* (**E**) roots from 6 days-old seedlings. DAPI staining of nuclei is shown in blue. Scale bar: 20 µm.

Fig S6, Related to Fig 6. Lateral root emergence in mutant and over-expression lines. (**A**) Percentage of emerged primordia out of the total number of initiated LRP in *pdbg1*, *pdbg2*, *pdbg1,2* and PdBG1OE in the Col background at 10 days post-germination. (**B**) Percentage of ‘emerging’ primordia after 42h gravi-stimulation. Seedlings grown for 3 days in vertical positioned plates containing 0.5xMS were subjected to gravi-stimulation as described by (Peret et al., 2012). The number of ‘emerging’ (stage VII) primordia from the total initiated in the outer area of the bend was quantified and expressed as a percentage. No significant difference was observed between wild-type and lines with altered PdBG expression. (C) stage VII primordia for wild-type and PdBG1OE 42h post-gravistimulation. Error bars represent standard deviation. Asterisks represent statistical significance: (**, P<0.01). Scale bar: 20 µm.

Table S1, Related to Fig 3. Gene expression analysis of callose metabolic enzymes identified in the proteome of purified PD-enriched cell walls. The table provides information on predicted activity, localization and expression for a set of BGLs (1,3 beta-glucanases) and GSLs (callose synthases) enzymes identified in the cell-wall and PD enriched proteome (Parizot et al., 2010; Fernandez-Calvino et al., 2011). Sheet1 explains the table legend. Sheet2 shows the results. Screening for proteins, present in the PD proteome, with preferential expression (highlighted in red) in the xylem-pole pericycle (XPP), responsive to NAA treatment and regulated by *slr1* identified *At3g13560 (PdBG1).* Expression of *PdBG1* close relatives *At2g01630 (PdBG2)* and *At1g66250 (PdBG3)* is also included. Note that, like *PdBG1, PdBG2* fulfils our criteria for selection.

Table S2, Related to Experimental Procedures. Primers used for PCR amplification in this study [a].

Cloning/Genotyping	Primer name	Sequence 5'-3'
Promoter of AUX1	attb1-pAUX1	GGGGACAAGTTTGTACAAAAAAGCAGGCTcaagttgattaaatttcatggatca
	attb5R-pAUX1	GGGGACAACTTTTGTATACAAAGTTGTaataaaacagagcgaaagaatcg
mCitrine-PdBG1	P1	GCTCGATCCACCTAGGCTgcactctgtttccaatgctg
	P2	CACAGCTCCACCTCCACCTCCAGGCCGGCCtgcgtttaagcttcccgtat
	P3	TGCTGGTGCTGCTGCGGCCGCTGGGGCCaacgctactaatggaaactttcctc
	P4	CGTAGCGAGACCACAGGActacaaaaggcggtcatgct
mCitrine-PdBG2	P1	GCTCGATCCACCTAGGCTatggctgcccttcttctc
	P2	CACAGCTCCACCTCCACCTCCAGGCCGGCCattgcttttgcacttccag
	P3	TGCTGGTGCTGCTGCGGCCGCTGGGGCCcagacacttggaaacaacacct
	P4	CGTAGCGAGACCACAGGActacaagaatactaaggcaatgatca
mCitrine-PdBG3	P1	GCTCGATCCACCTAGGCTatggcttctcttctccatcttc
	P2	CACAGCTCCACCTCCACCTCCAGGCCGGCCgctcccagcaaacacacat
	P3	TGCTGGTGCTGCTGCGGCCGCTGGGGCCcgcggtaatggtagaaacg
	P4	CGTAGCGAGACCACAGGAtcacaagatattagcaacgttca
Genotyping *pdbg*1	FWD	gcagctgcttgggttaacaa
	REV	gtctccgcattagcgactgt
Genotyping *pdbg*2	FWD	cacaccggggttcaagttat
	REV	ctgtgaccacgattggaatg
Genotyping *pdbg*3	FWD	cagcttctccttctcctcca
	REV	tgaagttgcaagcatcagga

(a) Linker sequences (for overlapping PCR or for recombination in the GATEWAY vector) are in uppercase.

Reference List

Fernandez-Calvino,L., Faulkner,C., Walshaw,J., Saalbach,G., Bayer,E., Benitez-Alfonso,Y., and Maule,A. (2011). Arabidopsis plasmodesmal proteome. PLoS. One *6*, e18880.

Parizot,B., De,R.B., and Beeckman,T. (2010). VisuaLRTC: a new view on lateral root initiation by combining specific transcriptome data sets. Plant Physiol *153*, 34-40.

Peret,B., Li,G., Zhao,J., Band,L.R., Voss,U., Postaire,O., Luu,D.T., Da,I.O., Casimiro,I., Lucas,M., Wells,D.M., Lazzerini,L., Nacry,P., King,J.R., Jensen,O.E., Schaffner,A.R., Maurel,C., and Bennett,M.J. (2012). Auxin regulates aquaporin function to facilitate lateral root emergence. Nat. Cell Biol. *14*, 991-998.

A

B

LRP

C

LRP

D

LRP

E

LRP

F

G

H

LRP

I

LRP

J

LRP

K

LRP

L

M

AUX1-YFP

N

O

P

Q

R

S

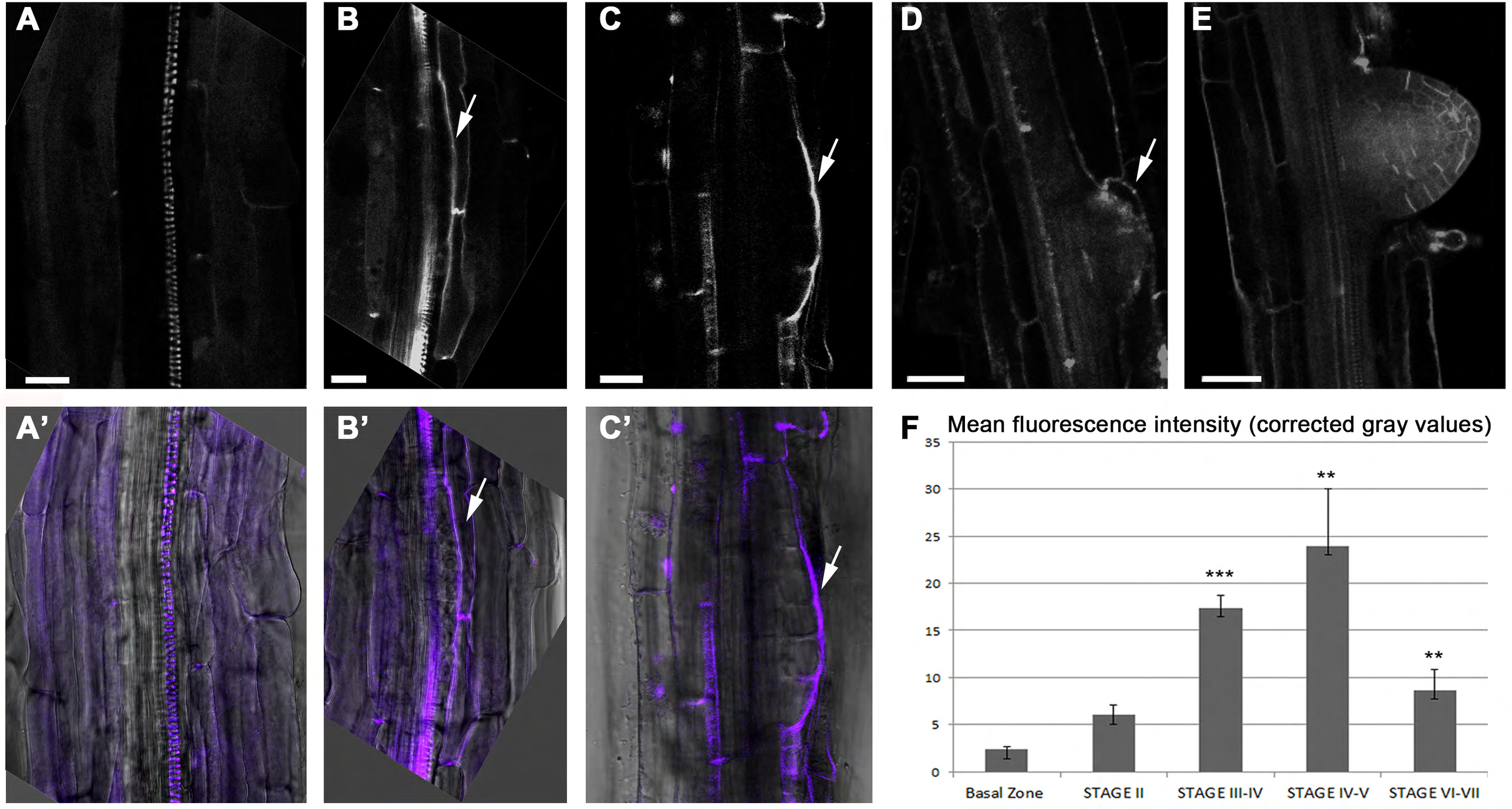
A
B
C
D
E
A'
B'
C'
F
Mean fluorescence intensity (corrected gray values)
35
30
25
20
15
10
5
0
***
**
**
Basal Zone
STAGE II
STAGE III-IV
STAGE IV-V
STAGE VI-VII

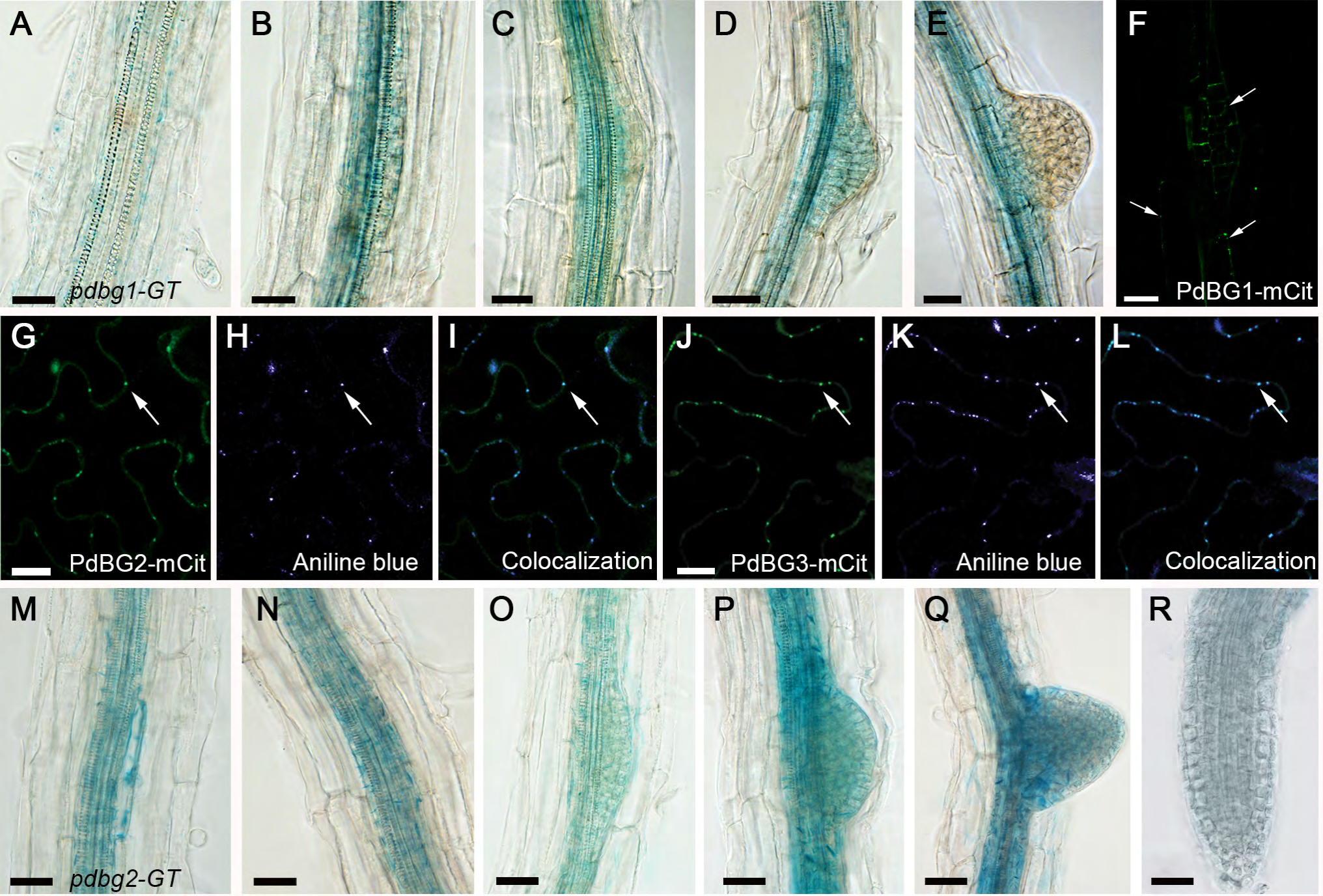
A
pdbg1-GT
B
C
D
E
F
PdBG1-mCit
G
PdBG2-mCit
H
Aniline blue
I
Colocalization
J
PdBG3-mCit
K
Aniline blue
L
Colocalization
M
pdbg2-GT
N
O
P
Q
R

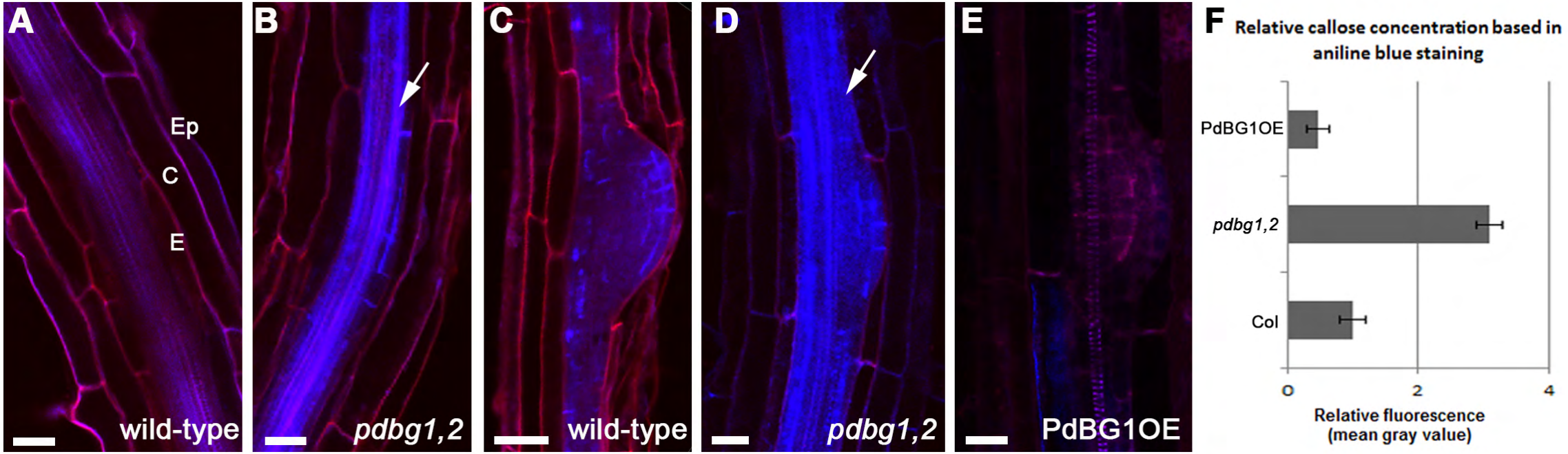
A
Ep
C
E
wild-type
B
pdbg1,2
C
wild-type
D
pdbg1,2
E
PdBG1OE
F
Relative callose concentration based in aniline blue staining
PdBG1OE
pdbg1,2
Col
0
2
4
Relative fluorescence (mean gray value)

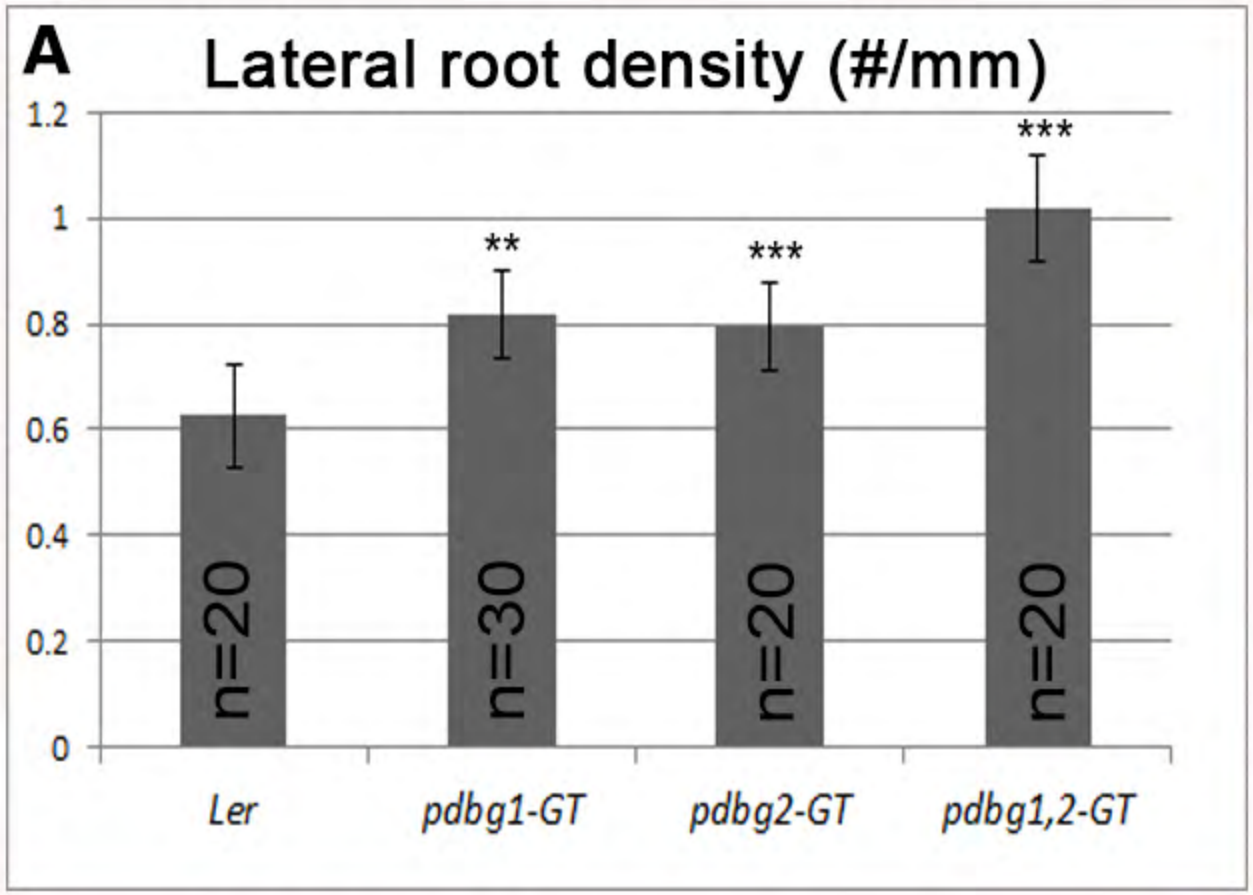
A
Lateral root density (#/mm)
1.2
1
0.8
0.6
0.4
0.2
0
**
***
***
n=20
n=30
n=20
n=20
Ler
pdbg1-GT
pdbg2-GT
pdbg1,2-GT


B
wild-type
PdBG1OE
pdbg1,2

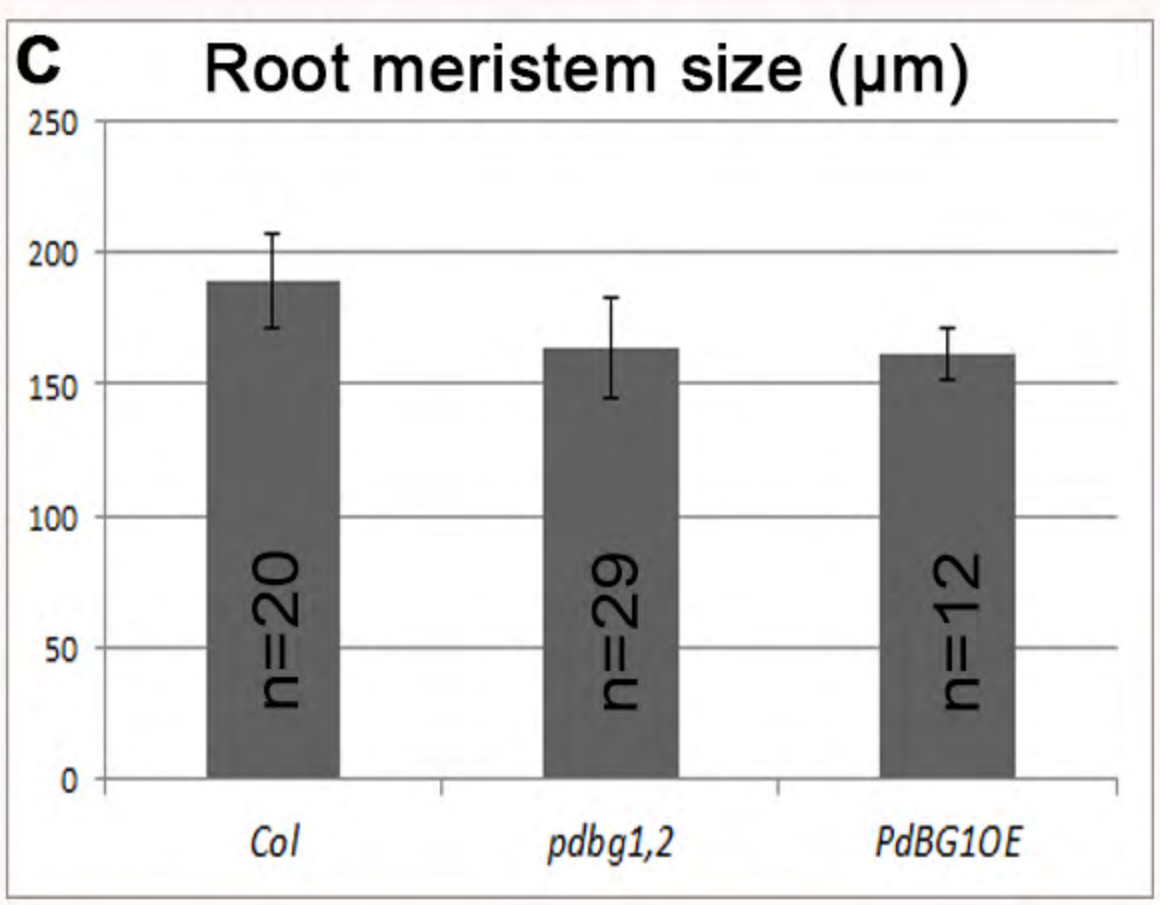
C
Root meristem size (µm)
250
200
150
100
50
0
n=20
n=29
n=12
Col
pdbg1,2
PdBG1OE

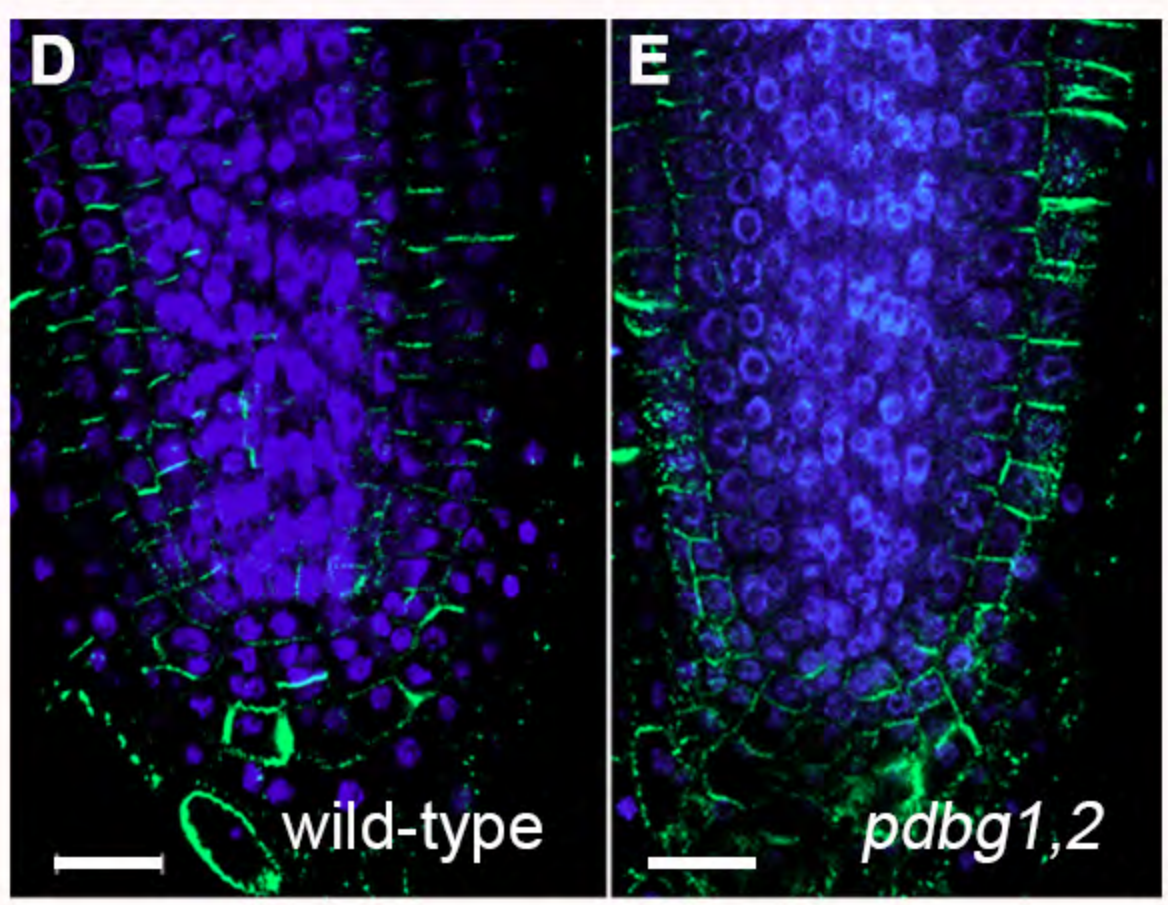
D
wild-type
E
pdbg1,2

A

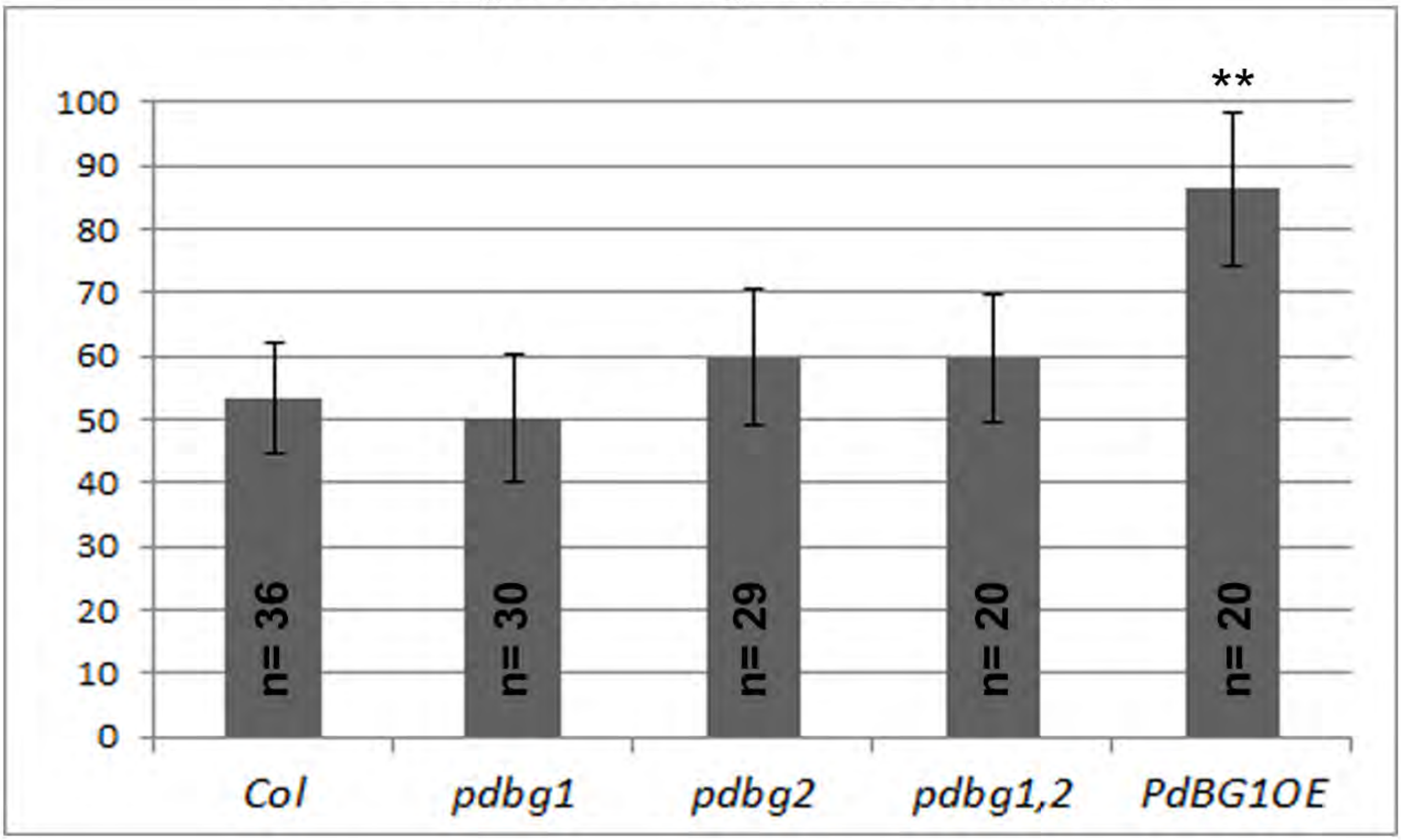
Percentage of emerged primordia (%)
100
90
80
70
60
50
40
30
20
10
0
**
n= 36
n= 30
n= 29
n= 20
n= 20
Col
pdbg1
pdbg2
pdbg1,2
PdBG1OE

B

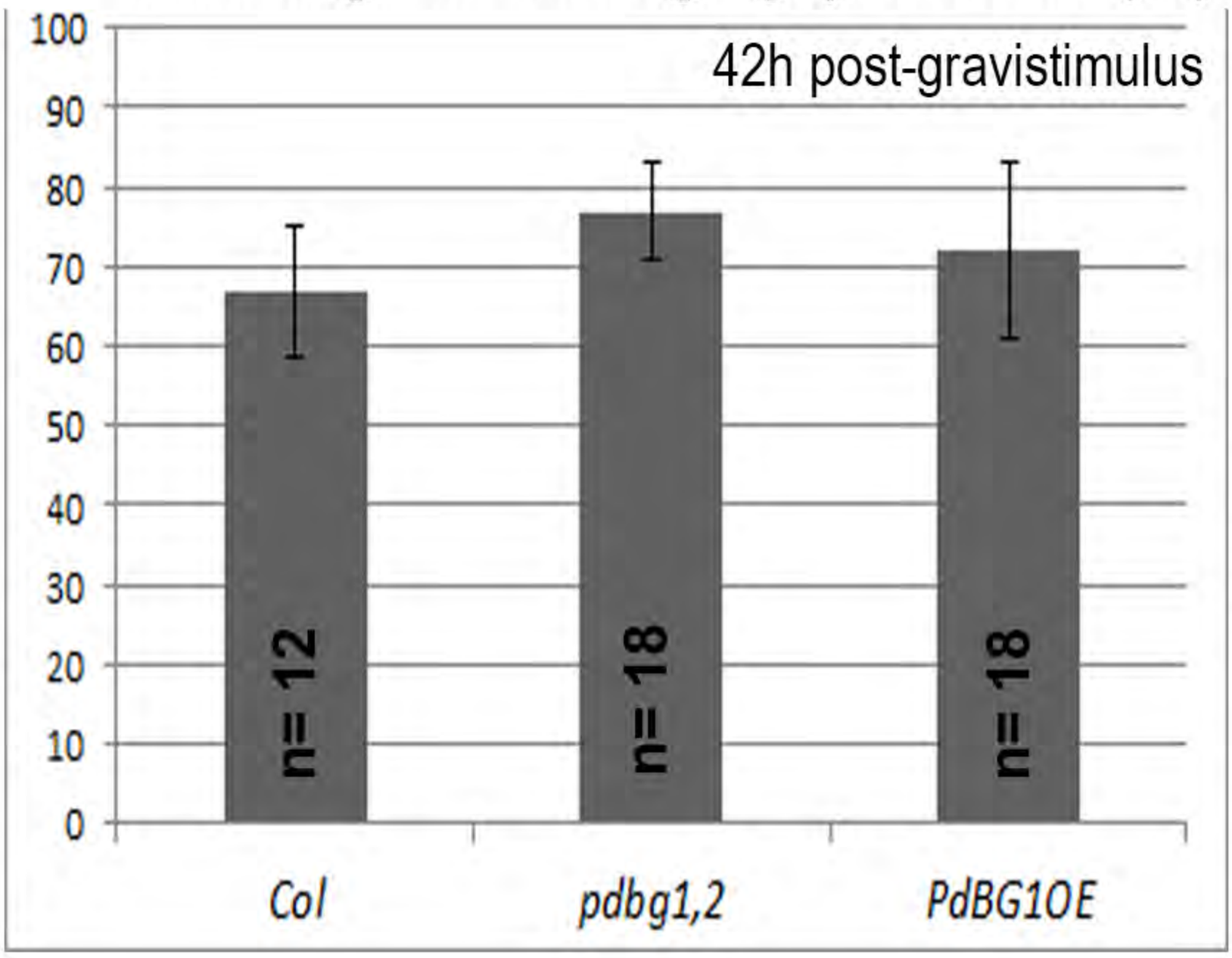
Percentage of 'emerging' primordia (%)
42h post-gravistimulus
100
90
80
70
60
50
40
30
20
10
0
n= 12
n= 18
n= 18
Col
pdbg1,2
PdBG1OE

C

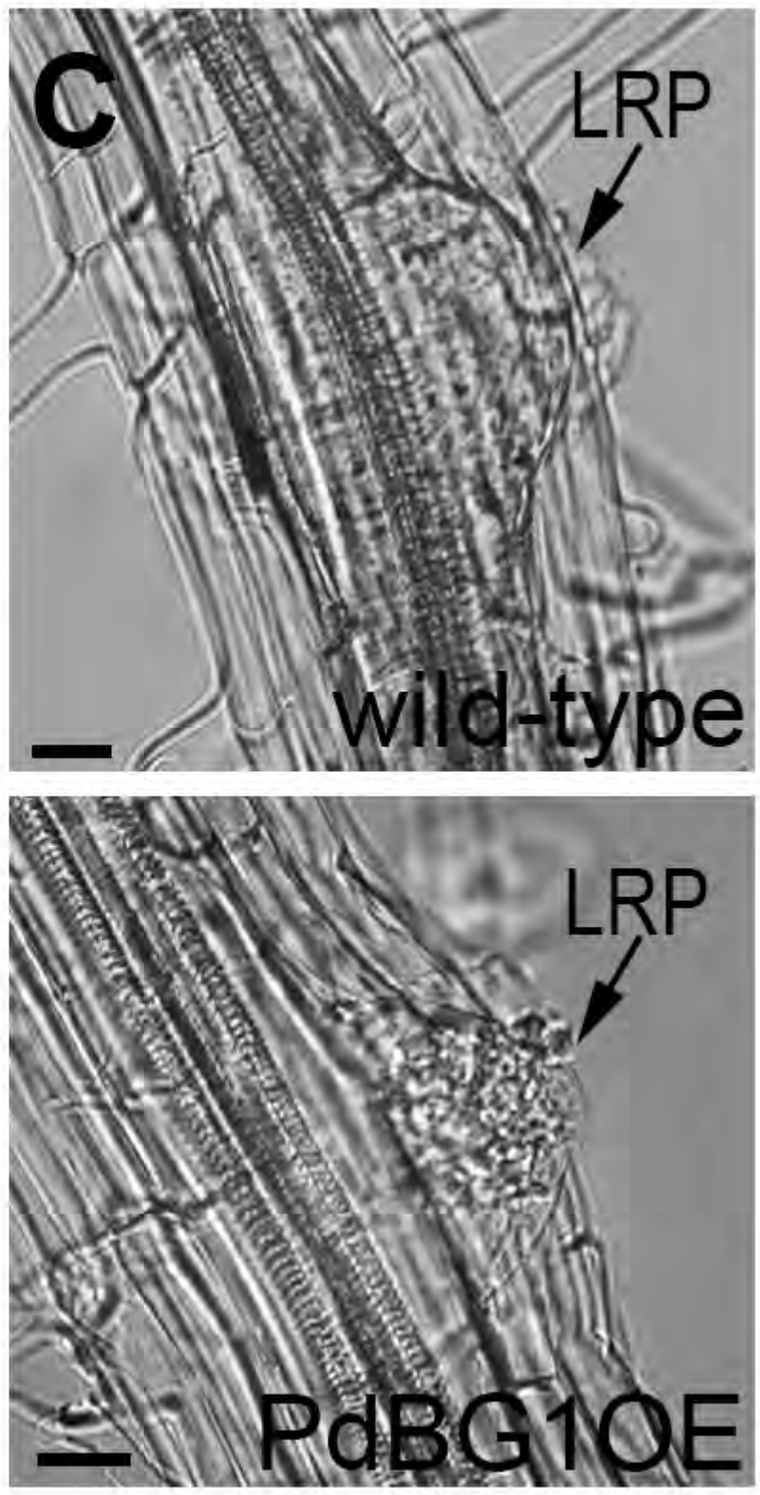
LRP
wild-type
LRP
PdBG1OE